Pure Appl. Geophys.

https://doi.org/10.1007/s00024-024-03555-4

Pure and Applied Geophysics

Continuous Gravity Observations at Campi Flegrei Caldera: An Accurate Assessment of Tidal and Non-Tidal Signals and Implications for Volcano Monitoring

U. Riccardi,[1,3] T. Pivetta,[2] A. Fedele,[2] G. Ricciardi,[2] and S. Carlino[2]

Abstract—We present the results of nearly one year of gravity recording acquired at the active caldera of Campi Flegrei (CFc). CFc is one of the three active volcanoes in the Neapolitan area (southern Italy) and is currently the most active one. In fact, the CFc is undergoing a period of unrest characterised by slow uplift of the ground, a peculiar phenomenon known worldwide as *bradyseism*, accompanied by seismicity and intense fumarolic emissions. Due to the increased intensity of the volcano dynamics, a permanent gravity station equipped with a gPhoneX spring gravimeter was installed to enhance the geodetic monitoring programmes. The purpose of the continuous recordings is to complement the time-lapse observations carried out periodically on networks of benchmarks, in order to continuously monitor the short-term gravity signals. We report on the various processing steps and analyses performed to obtain reliable parameters of the Earth's tides, non-tidal corrections and gravity residuals. The various methodologies employed to investigate the instrumental drift are also elucidated in depth, because it may masquerade the elusive gravity changes resulting from mass fluctuations within the volcanic and geothermal systems. Residual gravity signals, retrieved from the recordings, after reduction of body and ocean tides, polynomial drift, atmospheric, tilt and change of the Earth Orientation Parameters (EOP) effects, appear to be uncorrelated with hydrology, while they show a clear correlation with the most energetic earthquakes, that strongly characterise the current bradyseismic crisis. The residual gravity signals display peculiar trends characterized by steps or offsets (up to about 600 nm/s^2) and transients in coincidence of the most energetic volcano-tectonic events (Magnitude > 2.5) and seismic swarms. The steps in the gravity residuals are likely to be of instrumental origin, while the amplitudes of the observed transients are not consistent with co-seismic or volcanological phenomena, for which there is no evidence from other monitoring techniques. Unfortunately, the lack of repeated absolute gravity measurements severely limits our ability to attribute the observed gravity variations to geological sources. From the analysis of the gravity records, reliable tidal gravity models have been derived, which will improve the accuracy of volcano monitoring by allowing a precise reduction of tidal effects for both relative and absolute gravity measurements taken in these volcanic areas.

Keywords: Campi Flegrei, caldera, bradyseism, Unrest, continuous gravity records, volcano monitoring, gravity tides.

1. Introduction

1.1. Gravimetry for Volcano Monitoring

Because of its unique capability to detect mass and density change, microgravity is better suited than other geophysical or geochemical techniques for volcano monitoring in sensing magma or fluids accumulation or drainage. This is the reason why time-lapse gravimetry has been used for decades to better understand not only magmatic activity at volcanoes, but even to gain insight into the dynamics of subsurface fluids, like water and hydrocarbons (Forster et al., 2021; Mouyen, 2023; Pivetta et al., 2024; Portier et al., 2018; Sugihara et al., 2013). Microgravimetry has now become a traditional volcano monitoring technique. In fact, the use of repeated gravity surveys aimed at detection of small amplitude temporal changes in gravity, or "microgravity," for eruption forecasting dates back the 50's of last century. Iida et al. (1952) detected significant gravity increases of up to hundreds of μGal (1 μGal = 10^{-8} m/s^2 = 10 nm/s^2 = 10^{-9} g) before the eruption and decreases during the eruption of Izu-Oshima, Japan. The measured changes could not be fully explained by the levelling data, hence pre-eruptive mass increase and co-eruptive mass decrease had to be invoked depicting the dynamics of magma

Supplementary Information The online version contains supplementary material available at https://doi.org/10.1007/s00024-024-03555-4.

[1] Dipartimento Di Scienze Della Terra, Dell'Ambiente E Delle Risorse, Università Di Napoli Federico II, Naples, Italy.

[2] Istituto Nazionale Di Geofisica E Vulcanologia, Sezione di Napoli–Osservatorio Vesuviano, 80124 Naples, Italy. E-mail: tommaso.pivetta@ingv.it

[3] Research Group 'Geodesia', Universidad Complutense de Madrid, 28040 Madrid, Spain.

Published online: 05 September 2024

accumulation and drainage at depth. An exhaustive review on the use of microgravimetry in volcano monitoring can be found in de Zeeuw-van Dalfsen and Poland (2023).

Like other monitoring techniques, high-precision gravimetry has its strengths and weaknesses, but recently a hybrid approach has been gaining popularity. It consists of different forms of data collection (surveys and continuous) based on different types of gravimeters, relative (spring and superconducting) or absolute (ballistic and quantum). Such a hybrid approach offers the potential to record a wide range of signals from volcanoes in different dynamic states (quiescent or open conduit) with different plumbing systems. The need of multi-instrument networks is almost obvious when both the temporal and spatial resolution is needed for effective volcano monitoring. In fact, with relative gravity campaigns typically lasting a few days to weeks and then repeated years or months later (de Zeeuw-van Dalfsen & Poland, 2023; Pivetta et al., 2023), the spatial resolution of these studies is usually at the expense of temporal resolution, and vice versa. The joint use of relative monitoring networks with continuous gravity observations, with one or two instruments recording for short periods of time (from months to a few years) at selected sites, can bridge the gap. Moreover, including in the gravity monitoring infrastructure also the repetition of measurements with absolute gravimeters at permanent sites as well as at the reference station of the networks would have the double advantage of allowing to constrain the instrumental drift of the recording gravimeter, as well as to check the gravity stability in the site used as reference of the relative network. In summary, the state of the art shows that the most effective gravity monitoring of underground mass redistribution caused by any geodynamic phenomenon, including volcanism, is the multi-instrument, multi-mode hybrid system (Portier et al., 2018).

Continuous microgravity studies are not routinely performed on most active volcanoes; this is mostly due to high cost of the instrumentation necessarily set into a few selected points, leading to gravity observations at low spatial resolution. However, some long-term experiments with continuous gravity recordings have been performed on active volcanoes (e.g. Jousset et al., 2000; Riccardi et al., 2023) and have led to precise Earth tide models for the areas of Mt. Somma-Vesuvius (Italy) and Merapi (Indonesia), and have allowed the detection of rapid (minutes to days) mass redistributions and their interpretation in terms of volcanic activity (Carbone et al., 2006, 2008). The application of continuous gravity measurements to active volcanoes led to interesting results about the volcano dynamics and the magmatic processes occurring in the pre-eruptive phases as well as during the eruptions (Williams-Jones et al., 2008). For instance, gravity changes measured with the Micro-g LaCoste gPhone-054, occurring during the initial stage of the 2011–2012 El Hierro (Canary islands) submarine eruption, have been interpreted by Sainz-Maza Aparicio et al. (2014) as pre-eruptive signatures during the episode of unrest. A continuous recording of a spring gravimeter unveiled a change in gravity preceding the eruption at Kilauea in 2021 and 2023, as well as during a minor intrusion in 2023 (de Zeeuw-van Dalfsen & Poland, 2023). The week before the eruption in September 2021, a 3-day decrease in gravity of about 500 nm/s^2 (50 μGal) was recorded at a station located approximately 1 km east of the eruptive vent. The observed temporal pattern did not correlate with the deformation data, suggesting that the gravity variation was reportedly caused by mass redistribution. Carbone et al. (2023), from a joint analysis of high-precision continuous gravity measurements with two GWR iGrav superconducting gravimeters and ground deformation data, have unveiled the important role of pressure-driven gas exsolution and expansion in the volume change of magma chamber during Mt. Etna eruptions. From the analyses of continuous gravity records, Riccardi et al. (2023) also derived reliable tidal gravity model at Vesuvius and correlated gravity residual with rainfall peaks. Gravity ''steps'', i.e. sudden and permanent changes in gravity, were recorded simultaneously at two stations on Etna's summit equipped with LaCoste&Romberg spring gravimeters during local low-magnitude earthquakes (Carbone et al., 2009). These steps were interpreted as geophysical evidence of dynamic stress transfer between tectonic and magmatic systems at the local scale.

Here the focus is on the results of more than a year (13/1/2023–29/2/2024) of continuous gravity

observations using a gPhoneX at Campi Flegrei active caldera (Fig. 1) during the ongoing period of unrest.

1.2. *Campi Flegrei Caldera: Past and Current Unrest Episodes*

Campi Flegrei caldera is roughly 12 km wide and includes the city of Pozzuoli, in its centre, and a part of the city of Naples in its eastern sector. Inside this area, more than 450.000 people are exposed to the volcanic risk in case of a medium-size eruption (Carlino, 2019). The dynamics of the caldera is quite peculiar, characterised by recurrent episodes of slow ground motion with a predominantly vertical component, known worldwide as bradyseism, accompanied by seismicity and intense fumarolic activity during the uplift phase. In 1970–72 and 1982–84 the caldera showed clear signals of unrest with a cumulative ground uplift of more than 3 m, with its maximum close to Pozzuoli harbour, and escalating of seismicity starting from 1982 (Danesi et al., 2024). During the 1982–84 crisis, the seismic stations of the Osservatorio Vesuviano recorded more than 16,000 shallow volcano-tectonic (VT) earthquakes (with maximum duration magnitude Md = 4.0) (Del Pezzo et al., 1987; Petrosino et al., 2008), coinciding with a maximum uplift at Pozzuoli of about 180 cm (Danesi et al., 2024; Del Gaudio et al., 2010). After the 1984 a subsidence phase began and continued for about 20 years, lowering Pozzuoli by 93 cm (Del Gaudio et al., 2010). A new phase of unrest started in 2005 with a rate of uplift (maximum of few cm per months) about one order of magnitude lower than in the previous crisis. Significant increase of CO_2 emission at Solfatara (Fig. 1), a larger part of magmatic origin, has been recorded since the onset of the new uplift (Chiodini et al., 2021). By April 2022, the uplift had recovered the previous two decades of subsidence (Danesi et al., 2024) and it is still ongoing. Persistent seismicity returned in 2012–14, while it escalated starting from 2018 (Fig. 2). From

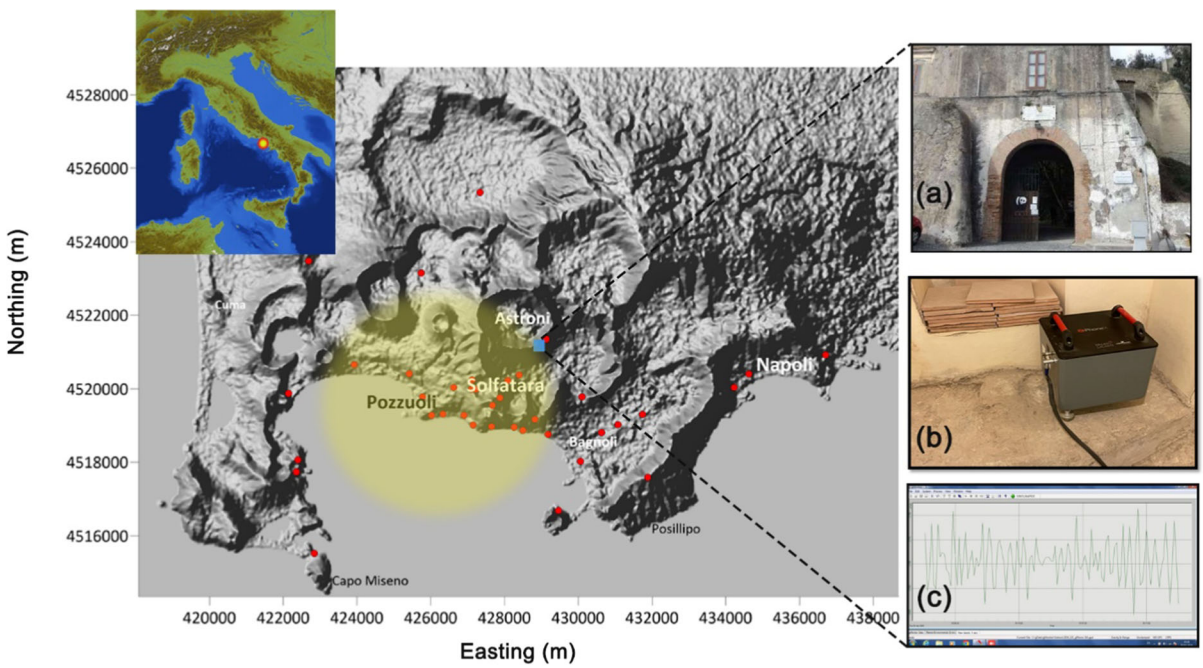

Figure 1
(Left) Campi Flegrei caldera with indication of the relative gravimetric benchmarks of time-lapse network (red points), the area involved in the largest ground uplift (yellow shadowed circle) (INGV-OV), the site of the gPh#116 gravimeter (blue square). Coordinate reference system: UTM33/WGS84. (Right) Details on the gravity permanent station: a) the entrance of the building hosting the permanent gravity station, b) the gPh#116 in the storage room and c) a sample of raw gravity (1 s) signal

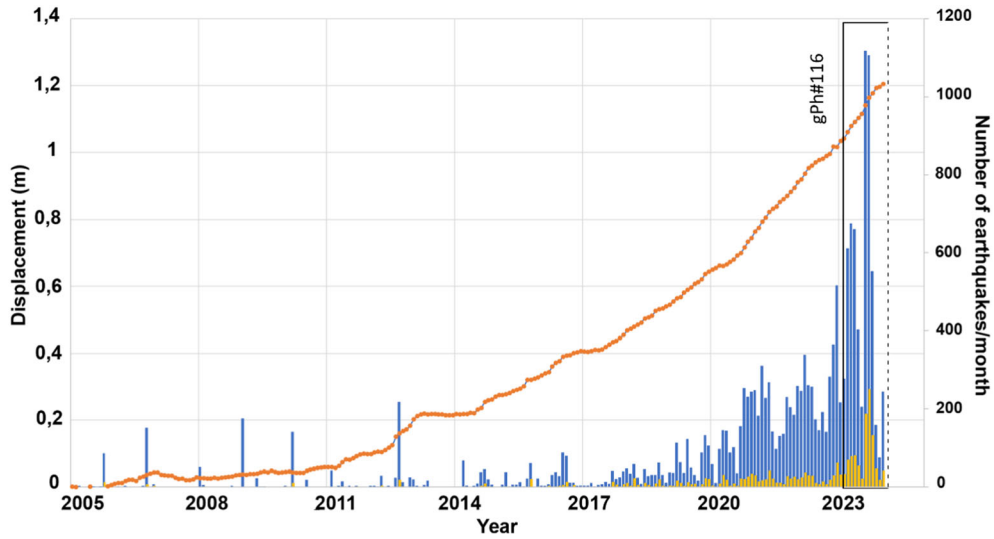

Figure 2
Maximum ground uplift recorded by the GNSS network (orange line; RITE station located in the centre of Pozzuoli) since 2005 and monthly number of earthquakes recorded by the INGV-OV seismic network (blue bars). Yellow bars are the monthly number of events with M $\geq$ 0.5 (Surveillance Bullettin INGV-OV, 2024). Black rectangle marks the temporal interval of the gravity recordings used for this study

2005 more than 6000 events with magnitude Md $\geq$ 0 and maximum magnitude Md = 4.4 have been recorded by the Istituto Nazionale di Geofisica e Vulcanologia, Osservatorio Vesuviano (INGV-OV) seismic network (Surveillance Bullettin INGV-OV, 2024).

The data related to gravity variation and ground deformation recorded during the 1982–84 crisis have been used by many authors which defined a "magmatic-type source", 3–4 km depth, as the cause of that unrest (e.g. Amoruso et al., 2008; Berrino, 1994; Bonafede et al., 2022; Trasatti et al., 2011). Using the same data, other authors (Gottsmann et al., 2006a, 2006b) proposed a possible hybrid source (fluids + magma), while Battaglia et al. (2006) found a solution for a source of 1982–84 unrest that is entirely composed by low density hydrothermal fluids. A debated and still open question is whether the present unrest is related to the overpressure of hydrothermal fluids and/or to magma movements in the shallow crust (3–4 km depth; Amoruso et al., 2014; Buono et al., 2022; Chiodini et al., 2021; D'Auria et al., 2015; Moretti et al., 2020). The response to this question is crucial in assessing the actual volcanic hazard of Campi Flegrei caldera and gravity measurements are essential in improving the understanding of caldera dynamic.

We use here data provided by 1 year of continuous gravity records between January 2023 and February 2024, at Campi Flegrei to elaborate an accurate gravity tide model for the area, which is important to attain a better correction of time-lapse gravimetry, routinely performed by INGV-OV. We also retrieve residual gravity signals to be interpreted to some extent in the light of the present-day dynamics of the Campi Flegrei caldera. In particular, the non-tidal gravity signals are compared with the ground deformations, the occurring seismicity and the meteoric recharge.

2. *Astroni Permanent Gravity Station*

For more than 40 years, INGV-OV has carried out an intensive geodetic monitoring programme mainly relying on NeVoCGNSS, a dense permanent GNSS network, supplemented with InSAR, tiltmetric and tide-gauge observations (De Martino et al., 2021; Polcari et al., 2022). Even the seafloor deformation is monitored in the marine sector of the caldera (De Martino et al., 2020). Time-lapse relative gravity

measurements are collected twice per year on a network of 36 benchmarks (Berrino et al., 1992). As enhancement of the geodetic monitoring programmes, in response to the increased intensity of the ongoing volcano dynamics, a permanent gravity station was installed in the most active central sector of the caldera (Fig. 1). In January 2023 the relative gravimeter gPhoneX#116 (hereinafter gPh#116) was installed at the WWF Nature Reserve of Astroni volcano, in the Campi Flegrei caldera. Before being installed at Astroni station, the gPh#116 was accurately calibrated, both in phase and amplitude, by intercomparison with two superconducting gravimeters and a FG5 ballistic gravimeter at J9 gravity observatory in Strasbourg (France) (Riccardi et al., 2023). The permanent gravity station is set in a small storage room, that is rarely accessed by visitors, located at the ground floor. The instrument package consists of a gPhone gravimeter, an UPS (Uninterruptable Power Supply), and a laptop computer running gMonitor software (Fig. 1b). Data storage, remote control, and adjusting of the gravimeter are allowed through the gMonitor software. The following data are collected and recorded at 1 Hz sampling rate: gravity changes, instrumental tilt levels, ambient temperature and air pressure, sensor temperature and pressure.

3. *Gravity Corrections: Theory and Analysis Methods*

3.1. *Data Processing*

The main objective of monitoring networks deployed in an active volcanic area is the early detection of precursors of renewed volcanic activity. In particular, the aim of any geodetic monitoring is to detect mass redistribution processes at depth associated with magma and fluids migration and the resulting ground deformation phenomena. A problem that arises when dealing with gravity, but more in general with potential field data, is the superposition of other different geophysical phenomena into the recordings, which may mask the target signals of interest related to mass variations of the volcano.

Hence our primary interest is to "residualize" the observed gravity recordings from all the non-volcano related signals that superpose their effects on the recording. Such effects are chiefly due to (1) body and ocean tides, (2) atmospheric pressure variations, (3) tilt variations and (4) instrumental effects, that include both drift and eventual tares and disturbances. Precise assessment of each of these contributions requires dedicated analysis and targeted processing of the acquired gravity data. Hereinafter we detail the various processing steps (flow chart in Fig. 3) used to separate and reduce these various gravity contributions which are then used to obtain the final gravity

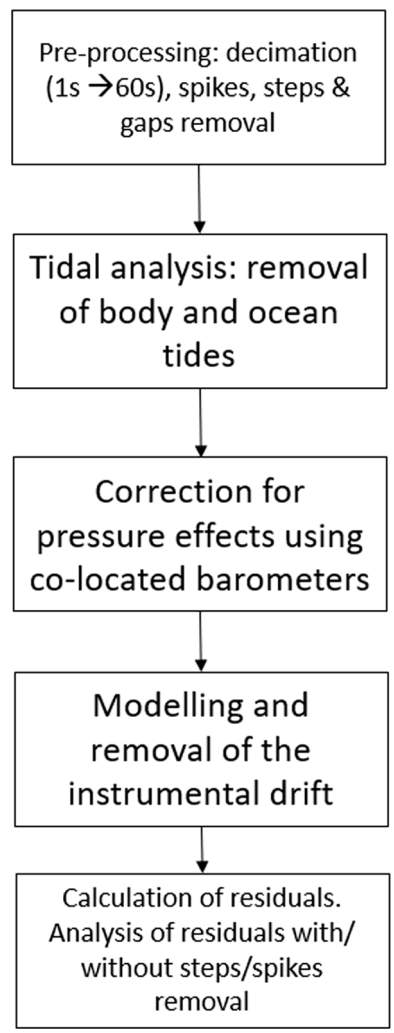

Figure 3
Flow chart illustrating the processing steps followed throughout this study

residuals. Theoretical background of the discussed geophysical effects and strategies to assess the quality and robustness of the corrections applied to our data are also reported in each of the following subchapters.

For all our analysis we take advantage of the gravity records collected during the period from 13 January 2023 to 29 February 2024. The original gravity observations are resampled from 1 to 60 s (1 min); before decimation data are low-pass filtered with a Finite Impulse Response filter, whose coefficients are optimized for ensuring no phase lags and a flat amplitude response especially in the tidal frequency bands.

3.2. *Body and Ocean Tides Contribution: Tidal Analysis*

A tidal analysis is performed on the full time series of 60 s gravity and pressure records using ETERNA-X (release ET34-X-V80) system for tidal analyses (Schüller, 2020). Before the analysis the gravity data are pre-processed, employing the so-called "remove-restore" technique. The "remove-restore" technique has the objective to "clean" the gravity data from all the contributions not related to tides and to atmospheric pressure variations. The procedure is done typically firstly removing from the original observations an initial guess model for tides, usually computed from the lunar-solar tidal potential with tidal gravimetric amplitude and phase factors retrieved from a previous tidal analysis performed at the same station (or from a theoretical model). Tilt effects (Δg_{tilt}) are removed using the well-known linearized approximation (cf. Riccardi et al., 2023):

$$\Delta g_{tilt} = g(1 - \cos\theta_x \cos\theta_y) \qquad (1)$$

where θ_x and θ_y are the calibrated tilt values of cross and long levels g is the absolute value of gravity at the location. The resulting tilt admittance is: $-4.9\ 10^{-3}$ nm/s^2/μrad^2. Atmospheric effects are also removed using a standard gravity pressure admittance, which amounts to -3.0 nm/s^2/hPa. This tidal-atmospheric corrected residual is then cleansed from short gaps, steps and spikes by visual inspecting the time-series and applying correctors through the TSoft software (Van Camp & Vauterin, 2005). Such clean residuals are then used to estimate the drift term (usually by piecewise juxtaposition of high order polynomials) and to remove it obtaining a new final residual. From this final residual, the subtracted tidal and atmospheric pressure effects are "restored", obtaining the gravity time-series input for the ETERNA program. Such a remove/restore of the pressure effect is only to allow the ETERNA system to assess more precisely the pressure admittance coefficient in the tidal analysis on the complete dataset. In the tidal analysis the atmospheric effects are adjusted through a single regression coefficient estimated by a least-squares fitting.

ETERNA is employed for estimating Earth and ocean tidal parameters (amplitudes and phases) and predicting tidal signals. Compared to its predecessor Eterna 3.40 (Wenzel, 1996), ET34-X-V80 reflects many important improvements for sophisticated analysis and retrieval of Earth information hidden in tidal observations. Readers can refer to the website (https://eterna.bkg.bund.de/) for a full description of the new features released as system variant ET34-x-v80-gnusim. The main objective of any tidal analysis performed on continuous records collected by permanent gravimeters is to obtain accurate tidal parameters, which characterise the Earth's response to the tides in the frequency domain. In fact, the Earth's tidal response is adequately represented by the gravimetric factors, also known as delta (δ), which is a dimensionless number, and phase leads (φ) for a given frequency. A concise definition of the delta can be the ratio of the vertical component of body tide measured by a gravimeter divided by the gradient of the external tidal potential along the perpendicular to the reference ellipsoid. Owing to the Earth inelasticity a small tidal phase lag (φ time delay) has to be also considered, which gives the delay of the tidal response with respect to the phase of the external tidal potential.

ETERNA allows also to account for the effects due to the variation of the Earth's Orientation Parameters (EOP), i.e. the polar motion (PM) and the variation of the length of day (LOD), amplified with a nominal delta factor 1.16.

To take into account the effect of the ocean tides we use ETERNA-X together with the calculation of the gravitational effect due to the ocean tidal loading

(OTL), freely available on the web (Bos & Scherneck, 2023), to perform the ocean loading correction. Six state-of-the-art models are considered: FES2014b, NAO.99b, EOT20, TPXO9.5a, CSR4.0, OSU2012 (Carrere et al., 2015; Eanes, 2002; Egbert & Erofeeva, 2002; Fok, 2012; Hart-Davis et al., 2020; Matsumoto et al., 2000).

3.3. Atmospheric Pressure Effects

For high-precision applications such as continuous and repeated monitoring, the magnitude of gravity effects induced by changes in atmospheric pressure can be significant. In fact, besides Earth tides, the atmosphere causes a significant contribution to time variable gravity measurements. Variations of up to several tenths of hPa in just a few hours can be recorded at some of the network's stations when baroclinic fronts pass through, corresponding to gravity variations of tens of nm/s^2 (few μGal), up to > 100 nm/s^2.

As the atmosphere circulation generates gravity signals with relevant amplitudes over a very broad spectral range, variations in atmospheric pressure can potentially inhibit the observation of small gravity signals of non-tidal origin produced by a range of geodynamic or hydrological phenomena. Accurate atmospheric corrections become critical to properly study certain volcanic or hydro-meteorological processes on specific time scales ranging from a few minutes to several days (Hector et al., 2014; Riccardi et al., 2008).

The simplest approach to reduce the atmospheric contribution in the gravity record is to use a single coefficient between local pressure and gravity, which can be nominal or derived experimentally from a regression analysis of gravity residuals against atmospheric pressure. In some tidal analysis codes, such as ETERNA-X (Schüller, 2020), this contribution can be calculated simultaneously with the adjustment of tidal groups.

When atmospheric pressure P (in hPa) is recorded jointly with gravity g (in nm/s^2) at a single station, the gravity can be reduced by using the relation:

$$g_r = g - \alpha(P - P_n) \tag{2}$$

where α is either a nominal value or determined by a least squares fit of P to g; P_n is a reference pressure at the station. As previously outlined, the nominal value of α is -3.0 nm s^{-2}/hPa and represents the resultant effect of pure attraction (-4.2 nm s^{-2}/hPa) owing to a Bouguer plate of the atmosphere, partially reduced by the loading effect, the latter is caused by the elastic deformation of the crust and the curvature of the Earth (Niebauer, 1988). In fact, this simple correction accounts for almost 90% of the atmospheric effect, which is largely sufficient for most time-lapse gravimetric applications for geodynamic purposes. More sophisticated approaches invoke frequency-dependent admittance, where the pressure effects depend on their frequencies and a set of complex admittance coefficients represent the transfer function of the atmospheric effect on the local gravity (Meurers, 2024).

The final step in pressure correction is to consider not only local pressure changes, but a pressure distribution around the gravity station, which may not be uniform, then requiring 3D atmospheric models. This leads to 2D or 3D loading computations including both Newtonian attraction and elastic deformation (Abe et al., 2010; Boy & Chao, 2005; Farrell, 1972; Spratt, 1982). A 2D approach results in a typical variability between -4.2 and -1.5 nms^{-2}/hPa in the near and far field, respectively (Hinderer et al., 2014). Some studies have also attempted to account for the spatial variability by using arrays of barometers (Riccardi et al., 2007) and others have shown that the admittance may vary as a function of time owing to seasonal fluctuations (Crossley et al., 2002).

In the context of managing the atmospheric noise in gravity measurements, one of the issues limiting the use of old spring gravimeters (i.e. Portable Earth Tide gravimeters manufactured by LaCoste&Romberg) for high-precision applications is the proven poor sealing of the core sensor, which tends to deteriorate over time inducing non-linear buoyancy effects to the beam. This invariably leads to inconsistent response of spring gravity meters to fluctuations in ambient pressure. Such a drawback apart from inducing a significant time modulation of gravity residuals, can even impact the accuracy of the

determination of some important diurnal (K1, P1 and S1) and semi-diurnal (S2, K2) waves.

On the contrary, thanks to the high sealing efficiency of the core sensor, the gPhone and the newest gPhoneX have proven (Microg-LaCoste, 2013) to be almost insensitive to humidity and buoyancy effects, allowing a consistent response of the instrument to external atmospheric pressure variations. In the following chapters we report on the assessment of the response of the gPh#116 to the external air pressure fluctuations both in time and frequency domain. We also check the temporal stability of the instrumental response.

3.4. Instrumental Drift: Theoretical Aspects and Relevance for Volcano Monitoring

It is well known that the main spectral feature of relative gravity time series, collected continuously or discontinuously with spring gravimeters, is that they are characterised by high energy at low frequency, so much so that many authors refer to this feature as the 'pink' spectrum (Riccardi et al., 2023). Such a spectral signature is caused by the instrumental drift. This is a thermo-mechanical effect on the elastic properties of the gravimeter spring, which even the housing of the critical elements in an evacuated chamber, does not fully eliminate. Furthermore, the elastic properties of the spring are not perfectly linear but exhibit a gradual creep over time (Long & Kaufmann, 2013). Indeed, instrumental drift can mask, if not hide, real gravity variations over time due magma and/or fluids motion. Therefore, the ability to model the instrumental drift becomes a crucial issue to be addressed. The correct separation between apparent variations of instrumental origin, i.e. drift, and real variations is crucial. From this point of view, superconducting gravimeters offer an undeniable advantage owing to their very low drift (a few tens of nm/s^2/year) with respect to spring gravimeters. For this reason, the use of superconducting gravimeters would be desirable for monitoring an active volcano, especially in case of rapid evolution of the unrest.

Hence the choice of gravimeter type is of paramount importance for monitoring purposes, given the peculiar drift characteristics. Typically, fused quartz gravimeters (like Scintrex CG5 or the newest CG6) have a relatively higher long-term drift than metal springs, like gPhoneX, LaCoste & Romberg or ZLS, but it is linear enough, then easy to be electronically compensated for surveying applications (Hugill, 2021). In fact, quartz sensors outperform in surveying gravimeters as they are virtually tare-free during transport and do not need to be mechanically clamped when moved from one site to another, which makes them sufficiently accurate as well as faster and easier to use than metal spring sensors. On the contrary metal spring sensors have lower long-term drift, which makes them better suited for stationary measurements. However, they are more susceptible to tares during transport because the elastic properties of their elastic suspension materials are lower than those of quartz.

We have devoted considerable space in this study to the analysis of the instrumental drift of gPh#116 in order to explore this issue in more detail. In particular, as already observed in the previous installation of the gPh#116 at Mt. Somma-Vesuvius (Riccardi et al., 2023) and from the experience of other authors (Fores et al., 2019), the characteristic behaviour of the instrument is such that when it is disturbed, either mechanically (shaking caused by a strong earthquake, intervention by an operator or disturbances at the station) or thermally (cooling of the instrument after a power failure), the instrument exhibits an instrumental drift of noticeable amplitude and strongly non-linear; some authors refer to it as "relaxation" (see Fores, 2019). Understanding whether these long-term variations are due to changes in drift and/or to real mass variations is fundamental. Hence in order to discriminate between these two options, we analyze the long-term gravity variations together with a database of "events", namely earthquakes and other documented disturbances (i.e. power failures, maintenance works in the building…). To fully characterize the drift and its changes after one of these events we employ different statistical approaches, in particular windowed regression analysis and polynomial fitting.

4. Results

4.1. The Tidal Analysis, Ocean Tide Loading and Near Diurnal Free Wobble

Considering the length of the available gravity record collected at the Astroni station (about 400 days), 45 tidal groups are reliably retrieved in terms of δ and φ. The longer than annual duration of the gravity records allows the reliable resolution of some individual waves in the diurnal tidal band (P1S1K1), whose amplitude is relevant for the latitude of Campi Flegrei. The results for the largest amplitude tidal waves are given in Table 1; the complete list of tidal parameters estimated using the ETERNA-X is provided in the supplementary material (S1).

To provide an insight into the quality of the results, in addition to the tidal parameter values, some statistical indices are also provided, such as Root Mean Square Error (RMSE), Signal to Noise Ratio (S/N) and Correlation RMSE Amplifier (CRA). As defined by Ducarme and Schüller (2018), the CRA is a quality measure of the effect of correlations due to record length and hence resolution. It indicates the increase in RMSE of the parameters owing to correlations. The RMSE of the computed tidal parameters is a function of the dataset length (N) and decreases with increasing N by $1/\sqrt{N}$. This means that if any two correlated harmonic signals have to be resolved from a gravity dataset of sufficient length, i.e. if the Rayleigh criterion is met, the CRA will be close to 1, so the correlation will not matter. In general the statistical outcomes of the tidal analysis demonstrate a robust determination of the tidal parameters, with a general S/N ratio that is higher than 30 dB.

Hereinafter we approach a detailed study on the ocean loading in the Campi Flegrei area. Figure 4a shows the results of the OTL correction applied to the 8 largest diurnal and semi-diurnal tidal waves as well as to the best resolved long period wave (Mf) at Astroni station.

As a measure of the efficiency of the OTL correction, the final residual phasors are calculated too (Fig. 4c). Following the notation shown in the Fig. 4b, the final residual phasor, X, is defined here as the remaining difference between an observed tidal harmonic (A) and the total theoretical tidal gravity calculated by combining the theoretical body tide (R)

Table 1

Results of the tidal analysis using ETERNA-X on the complete 410-day data set: delta factor and phase (phi) for the main waves. Root Mean Square Error (RMSE) on the parameters and signal-to-noise ratio (S/N); F is the frequency, A stands for the observed amplitude R is the amplitude for the non-hydrostatic, inelastic Earth model (WDZ-NHi)

Wave	F (°/h)	R (nm/s^2)	A (nm/s^2)	delta	RMSE	phi (°)	RMSE (°)	CRA	S/R (dB)
Mf	1.0980	17.91486	20.65435	1.15	0.03	−0.3	1.656	1.00	30.78
Q1	13.3987	58.84133	67.46495	1.1466	0.00034	−0.10	0.017	1.00	70.53
O1	13.9430	307.3207	353.0005	1.14864	0.00007	0.279	0.003	1.00	84.7
NO1	14.4967	24.15778	27.90357	1.1551	0.00073	0.1	0.036	1.00	64.01
P1	14.9589	142.9732	163.5113	1.14365	0.00017	0.034	0.009	1.02	76.42
S1	15.0000	3.37776	2.54253	0.75	0.0105	−29.6	0.799	1.02	37.11
K1	15.0411	432.0485	490.0956	1.13435	0.00006	0.3	0.003	1.21	85.38
PSI1	15.0821	3.37931	4.1235	1.220	0.00702	1.0	0.33	1.02	44.8
PHI1	15.1232	6.15057	7.02257	1.142	0.00407	0.6	0.204	1.02	48.95
TET1	15.5126	4.62129	5.31255	1.150	0.00472	0.6	0.235	1.05	47.73
J1	15.5854	24.16615	28.04607	1.1606	0.0009	0.04	0.044	1.00	62.20
OO1	16.1391	13.21517	15.25009	1.154	0.00103	0.1	0.051	1.00	61.01
N2	28.4397	82.34289	96.8785	1.17653	0.0002	1.23	0.01	1.00	75.52
NUE2	28.5126	15.64154	18.44396	1.1792	0.00098	1.65	0.048	1.00	61.62
M2	28.9841	430.0645	506.5477	1.17784	0.00004	0.924	0.002	1.00	90.36
L2	29.5285	12.15703	14.28099	1.1747	0.00081	0.45	0.04	1.00	63.23
S2	30.0000	200.071	234.5285	1.17223	0.00007	0.444	0.004	1.01	83.98
K2	30.0821	54.35003	63.80572	1.1740	0.00021	0.46	0.01	1.01	74.76
M3	43.4762	6.39516	6.74117	1.05	0.00211	1.3	0.115	1.00	53.95

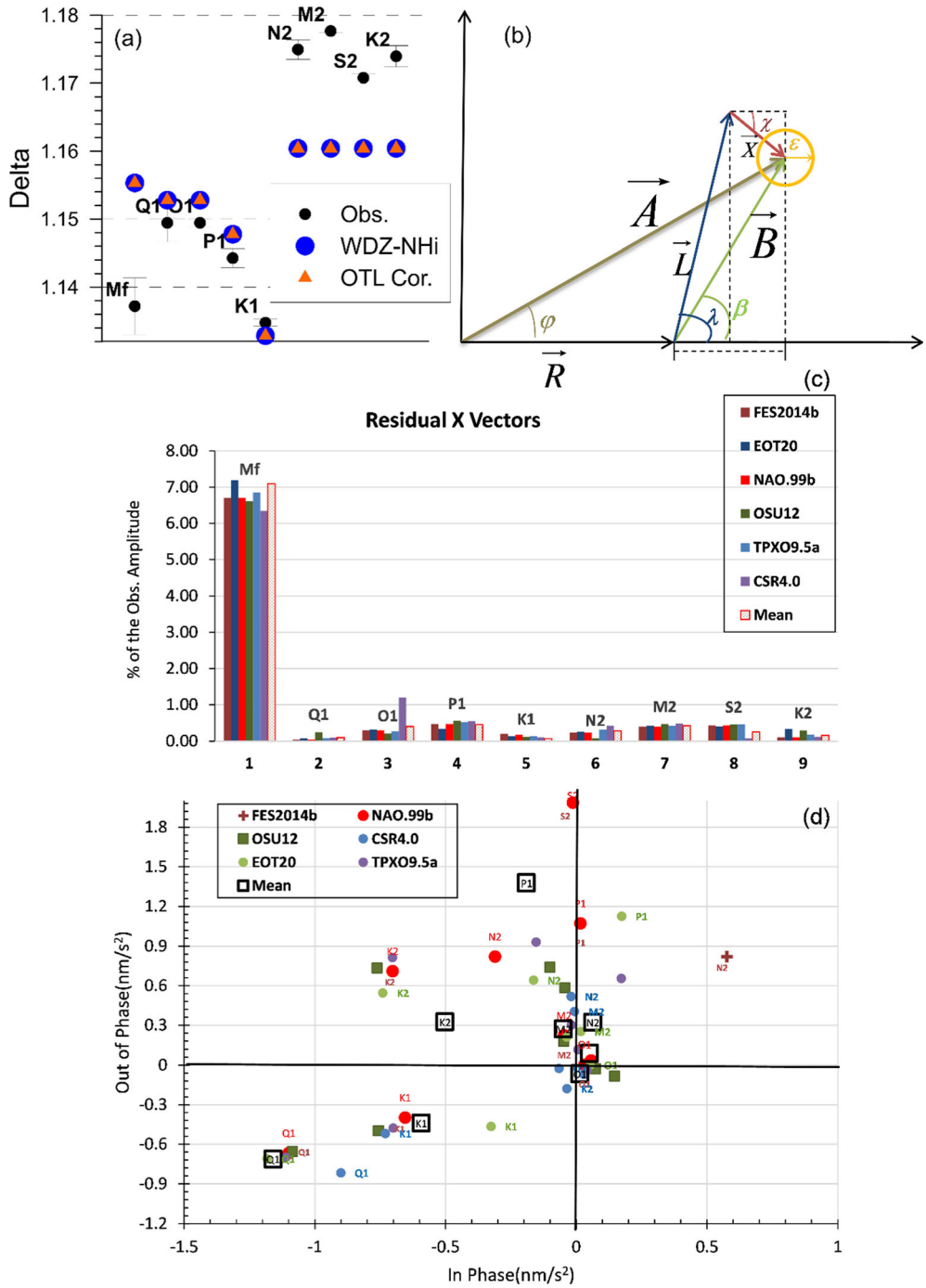

Figure 4

Ocean tide loading correction (OTL) of the delta factors according to FES2014b model (**a**). **b** Phasor plot employed in the OTL analysis: $\overrightarrow{A}$ is the observed tidal vector and its phase is φ $\overrightarrow{R}$ is the theoretical tidal vector according to a reference Earth model (WDZ-NHi). = $\overrightarrow{B}\overrightarrow{A} - \overrightarrow{R}$; β being the phase of $\overrightarrow{B}$. $\overrightarrow{L}$ is the Ocean tide loading from models and its phase is λ. $\overrightarrow{X}$= $\overrightarrow{B} - \overrightarrow{L}$ is the final residual vector and its phase is χ. ε reports the estimation of uncertainty on $\overrightarrow{X}$. **c** Amplitude of the final phasor residuals and in-phase and out-of-phase residuals after correction with 6 OTL models and the mean values of the models (**d**)

with the loading and attraction calculated using a particular OTL model (L):

$$X = A - R - L \tag{3}$$

where $\boldsymbol{A}$ is obtained from the tidal analysis, R is the body tide of a reference earth model, in this case the non-hydrostatic, inelastic Earth model (WDZ-NHi) (Dehant & Zschau, 1989; Wahr & Bergen, 1986), and L is the ocean tide loading from the web provider (Bos & Scherneck, 2023).

The amplitude of the residual phasors is rather small, less than 1% of the observed amplitude, which can be considered more than satisfactory for a spring-based gravimeter, at least for the main diurnal and semi-diurnal bands. The relatively large residuals of Mf, which remain below 10%, are certainly due to the unmodelled drift that strongly characterises spring gravimeters. In fact, the determination of Mf is at the limit of statistical significance. There are no relevant differences between the selected OTL models, indicating that the performance is more or less the same.

As the phasors X are complex valued they can be split in two components, in-phase (real) and out-of-phase (imaginary). The real component is routinely useful to get insights into calibration issues in amplitude, while the out-of-phase is related to the phase calibration.

The residuals are not randomly distributed around the origin (Fig. 4d). There is a greater spread of the diurnal waves along the in-phase axis, particularly for Q1 and K1 waves, the first is quite small (about 60 nm/s^2) at Campi Flegrei, while K1 could be affected by thermal influences as the station is set in a surface laboratory where significant daily temperature variations occur. On the contrary, the scatter along the out-of-phase axis is much smaller, except for S2, indicating that the instrumental phase shift caused by feedback, filters and the data acquisition system is relatively well determined. The S2 discrepancy could be a consequence of an incomplete pressure correction in the 12 h period, where the atmospheric pressure has a high spectral energy at mid-latitudes.

The high quality of the tidal analysis is also demonstrated by the clear evidence of resonance phenomena in the diurnal band, which is well resolved (Fig. 5a). It is well established that due to a misalignment of the axis of rotation of the elliptical fluid core with respect to the axis of rotation of the mantle, the Earth exhibits a rotational eigenmode called Free Core Nutation (FCN). This mode has a resonant period close to 430 sidereal days, while in a terrestrial rotation frame it is nearly diurnal, this is why the authors refer to it as Nearly Diurnal Free Wobble (NDFW). The existence of the NDFW has been repeatedly confirmed because it resonantly amplifies nearly diurnal tides. In fact, thanks to the resonance effects FCN is detectable in VLBI observations (Rosat & Lambert, 2009) as well as in the diurnal tidal waves, retrieved from some recording sensors such as gravimeters, tiltmeters and strainmeters (e.g. Cui et al., 2018; Amoruso et al., 2012; Riccardi et al., 2016). The main challenges in detecting the NDFW resonance in the tidal analysis stem from the frequency proximity of the individual constituents of the diurnal tidal band (P1, K1, PSI1, PHI1), which requires very long time series ($>$ 1 year) for adequate spectral resolution, and the weak amplitude of the PSI1 which is the closest in frequency to the resonance. The low amplitude harmonics like PSI1 and PHI1, are not accounted in the ocean models, but only the main diurnal waves (O1, Q1, K1, P1). As suggested by Merriam (1994), assuming that the ocean response to tidal forces is quite smooth with the frequency, the OTL correction for the minor diurnal waves can be retrieved from the so-called admittance by interpolation within the frequency bands. Indeed, the influence of the different OTL models for the minor tides does not have a large influence on the NDFW parameters (Merriam et al., 1994). The ocean tide correction is relatively small at Campi Flegrei; for diurnal waves it is about 0.2% of the delta factor and 0.5% in amplitude.

Figure 5b displays the good agreement between the observed delta factors, corrected for the OTL effect, and the theoretical spectrum of the resonance computed (according to Eq. 24 in Dehant et al., 1999) for hydrostatic (DDW-H) and non-hydrostatic (DDW-NHi) non-spherical rotating Earth (Dehant et al., 1999).

It is unrealistic to go beyond the simple detection of NDFW, so we will not attempt to estimate the parameters, i.e. period and quality factor of the resonance, either because of the length of the time

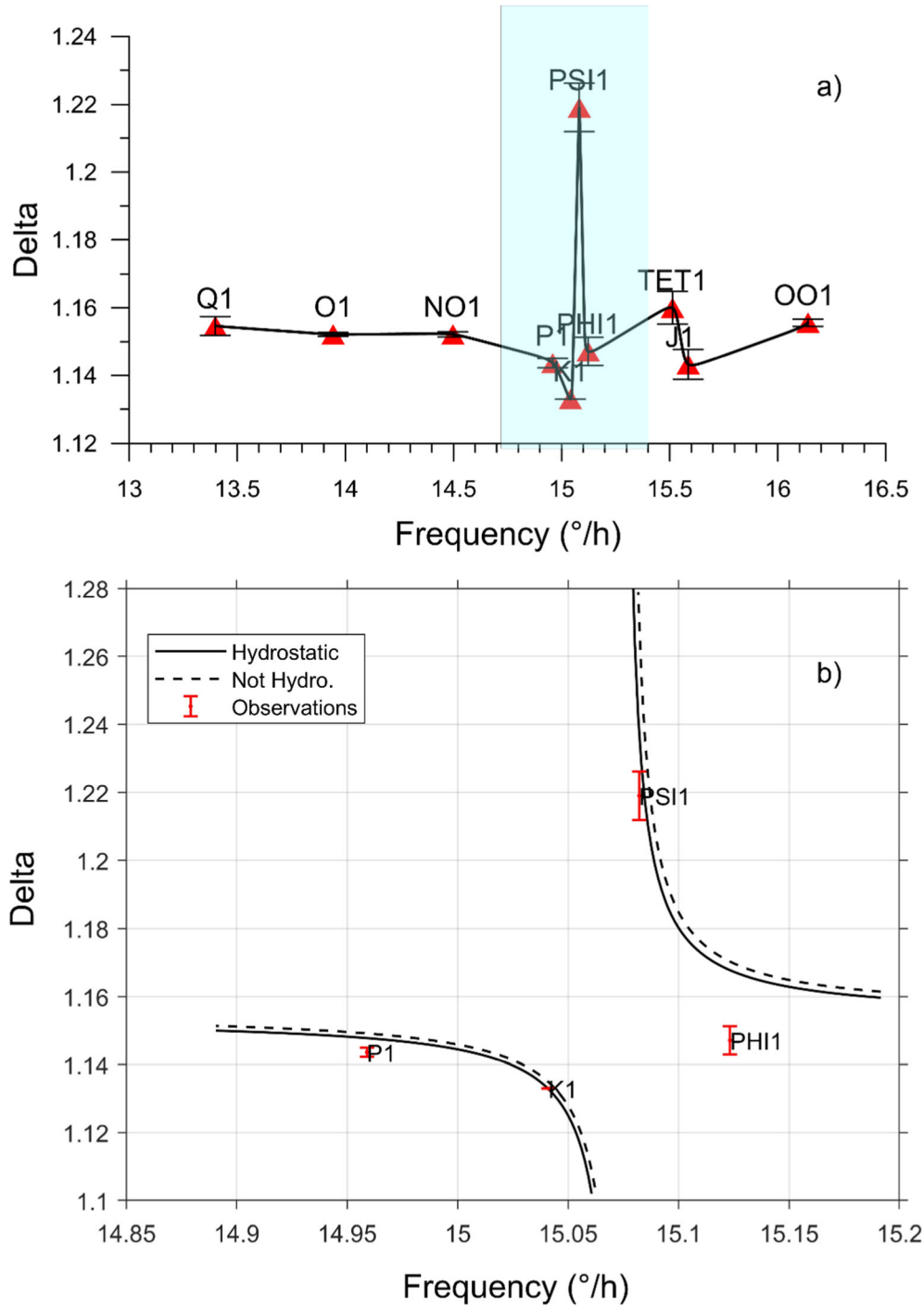

Figure 5
Effect of the Near Diurnal Free Wobble (NDFW) in the diurnal tidal band observed at Astroni gravity station (**a**); the cyan rectangle marks the frequency range shown below (**b**); observed delta factors and theoretical spectrum of the resonance computed for two hydrostatic and non-hydrostatic DDW models (**b**); frequency is in degrees per hour

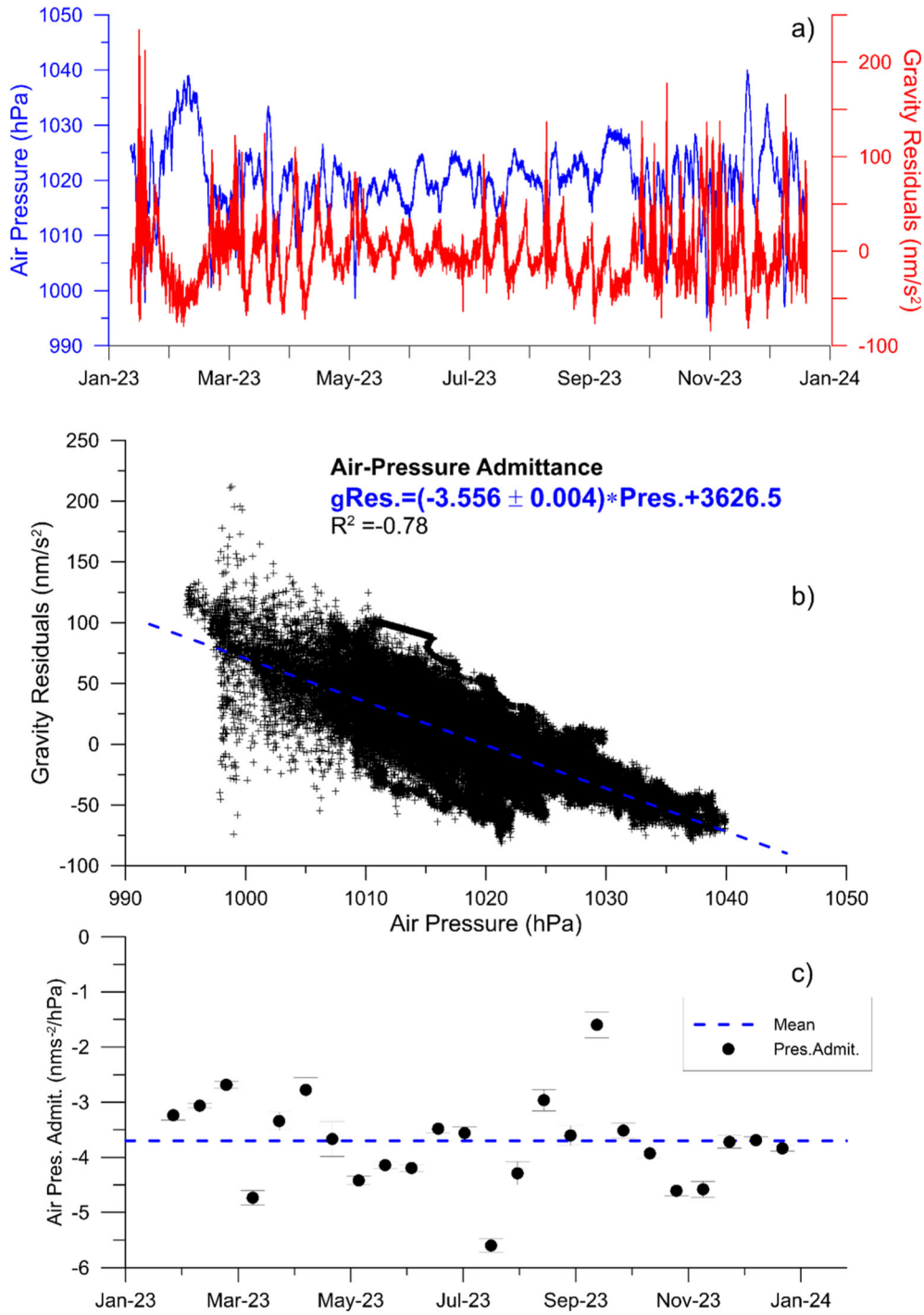

Figure 6
Atmospheric pressure admittance in the time domain: residual gravity and atmospheric pressure (**a**); Least-squares linear regression gravity vs. pressure with indication of the statistics (**b**); time evolution of pressure admittance coefficient in sets of 240 hourly samples (**c**)

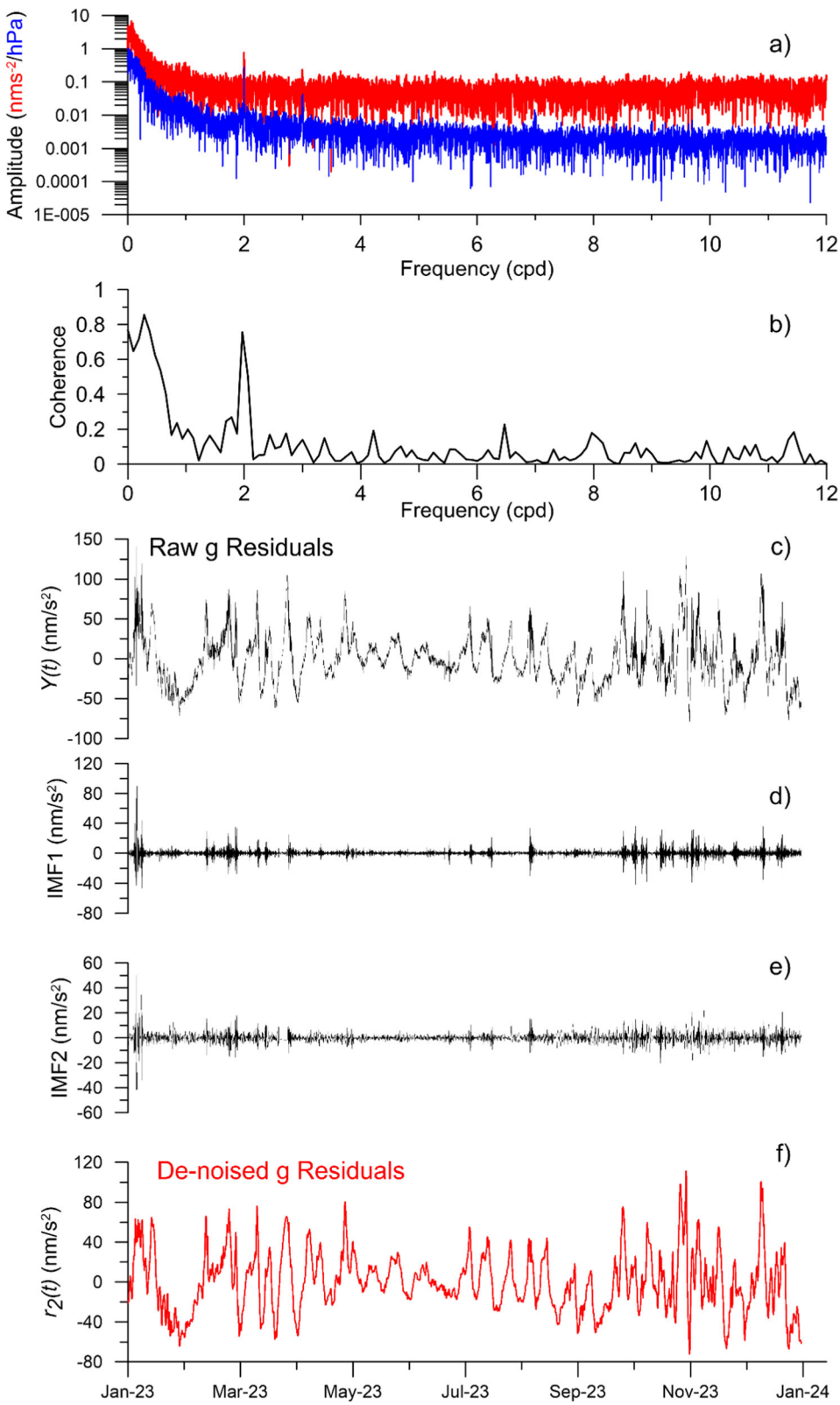
a)
Amplitude (nms-2/hPa)
10
1
0.1
0.01
0.001
0.0001
1E-005
0
2
4
6
8
10
12
Frequency (cpd)
b)
Coherence
1
0.8
0.6
0.4
0.2
0
Frequency (cpd)
c)
Raw g Residuals
Y(t) (nm/s2)
150
100
50
0
-50
-100
d)
IMF1 (nm/s2)
120
80
40
0
-40
-80
e)
IMF2 (nm/s2)
60
40
20
0
-20
-40
-60
f)
De-noised g Residuals
r2(t) (nm/s2)
120
80
40
0
-40
-80
Jan-23
Mar-23
May-23
Jul-23
Sep-23
Nov-23
Jan-24

◀Figure 7
Spectral analysis (**a**) and spectral coherence (**b**) of gravity residuals and air pressure, empirical mode decomposition (EMD) of the raw gravity residuals (**c**) by means of two intrinsic mode functions (**d**, **e**); de-noised gravity residuals (**f**)

series, which is at the limit of spectral resolution, or because of the general quality of the data obtained with a spring gravimeter, whose stability is severely undermined by drift.

4.2. The Atmospheric Pressure Admittance

Since here we are only interested in the response of the gravimeter to changes in ambient pressure, the gravity signals need to be 'cleansed' of all tidal, tilt and drift effects as much as possible. We remove tidal effects using a synthetic time-series derived from tidal analysis. Tilts and drift effects are corrected as well; as for the drift we employ a piecewise polynomial model that fits the long term gravity variations (details in the following chapter 4.3). The obtained residuals used for the atmospheric pressure analysis are shown by the red curve in Fig. 6a. The ambient pressure admittance is recovered from the least squares linear regression of the gravity residuals versus the atmospheric pressure (Fig. 6b). The larger scattering when the barometric pressure values are low is evident (Fig. 6b); this is a clear effect of bad weather conditions inducing larger noise on gravity signals. The obtained admittance coefficient (-3.556 ± 0.004 nms^{-2}/hPa) is reasonably close to the expected nominal value. Similar results (-3.16 ± 0.084 nms^{-2}/hPa), considering the larger estimated errors, are obtained from tidal analyses performed with the ET34-X-V80 software.

To study the temporal evolution, if any, of the admittance coefficient, a least squares regression analysis is performed by windowing the gravity residuals and the air pressure values in sets of 240 hourly samples (10 days) with an 80% overlap (Fig. 6c). The largest scattering of the admittance coefficients occurs during the period of intense seismic activity in August–September 2023. Indeed, any seasonal study cannot be done because the data set spans only one year.

The spectral analysis of the gravimetric residuals and the atmospheric pressure (Fig. 7a) clearly shows that the pressure has considerable energy at low frequencies (< 1 cycle per day, cpd), which is due to the fact that, at the latitudes of the study area, the meteorological systems are dominated by frontal systems linked to the cyclical establishment of cyclonic and anticyclonic areas, while at daily frequencies the signal with the greatest amplitude is at 2 cpd (12 h). This component is related to the cyclical insolation of the lower, denser layers of the troposphere. Coherence analysis confirms that atmospheric pressure significantly influences the gravimetric residuals and the that both the gravity residuals and pressure in the Astroni station remain strongly coherent up to frequencies of 3 cpd, with a maximum peak at 2 cpd (Fig. 7b). At higher frequencies (> 3 cpd) the signals lose coherence, most likely due to the high noise level of the gravimetric signal. Given these spectral and coherence characteristics, we decide to attenuate the high frequency noise before proceeding to determine the frequency dependent admittance. In particular, on the gravity residuals an Empirical Mode Decomposition (EMD) is applied (Huang et al., 1998). This decomposition is implemented in Matlab® and returns the "intrinsic mode functions" (IMF) and "residual" signal, where "residual" corresponds to the empirical mode decomposition of gravity residuals.

$$Y(t) = \sum_{i=1}^{N} IMF_i(t) + r_N(t) \tag{4}$$

where $Y(t)$ represents the "raw" gravity residuals (Fig. 7c). The denoised gravity residuals $r_2(t)$ (Fig. 7f) are retrieved from the transformation of the Eq. 4 by restricting the EMD to level 2 (i.e. not considering the modes shown in Fig. 7d and 7e), which is enough to reduce the high frequency noise in the gravity residuals as follows:

$$r_2(t) = Y(t) - \sum_{i=1}^{2} IMF_i(t) \tag{5}$$

The frequency-dependent admittance is nothing but a transformation of the Eq. (2) from the time domain to the frequency (ω) domain:

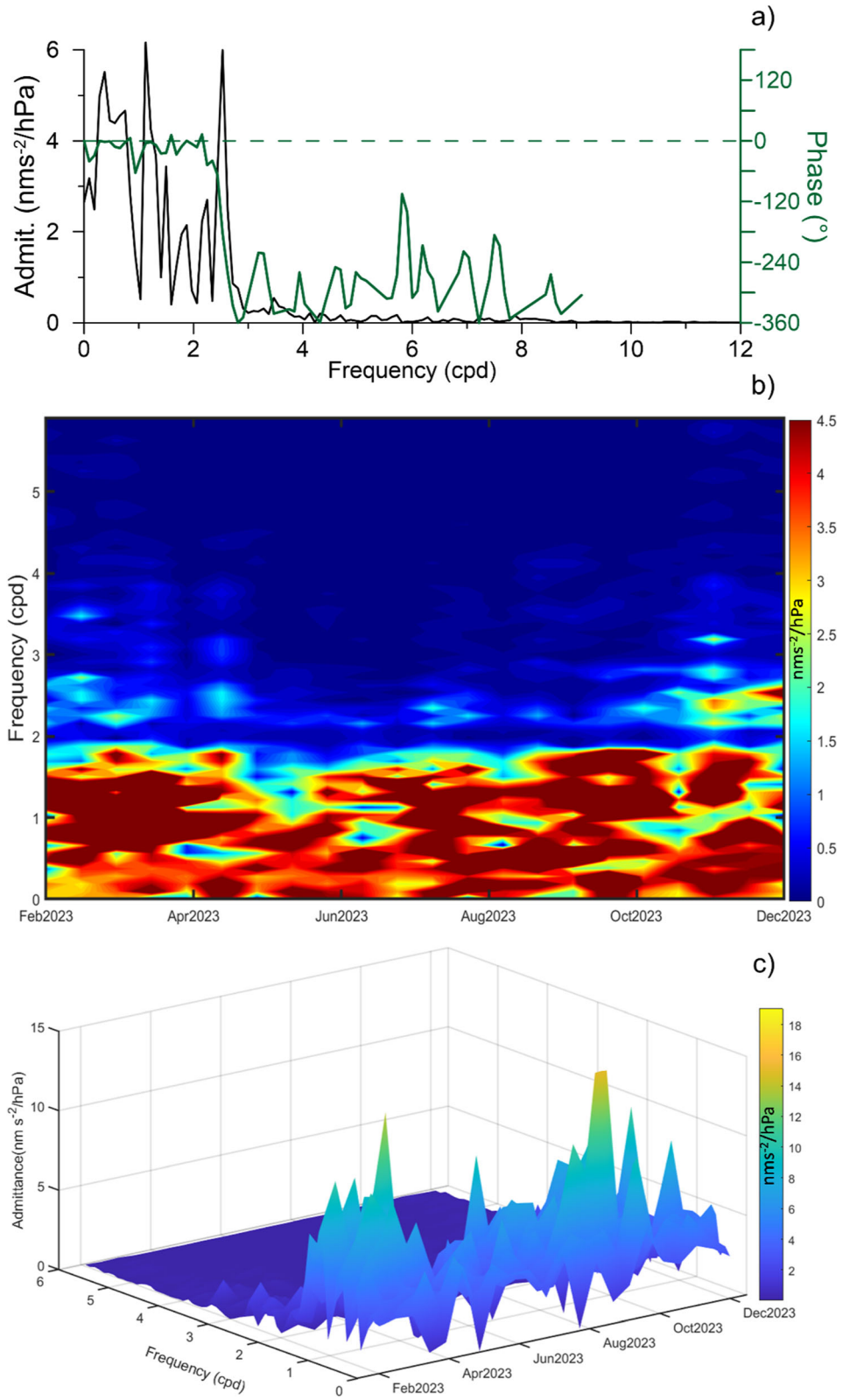
a)
Admit. (nms-2/hPa)
Phase (°)
Frequency (cpd)
b)
Frequency (cpd)
nms-2/hPa
Feb2023
Apr2023
Jun2023
Aug2023
Oct2023
Dec2023
c)
Admittance(nm s-2/hPa)
Frequency (cpd)
nms-2/hPa
Feb2023
Apr2023
Jun2023
Aug2023
Oct2023
Dec2023

◀Figure 8
Study of the pressure admittance in the frequency domain: frequency-dependent admittance in amplitude and phase (**a**); time evolution of the frequency-dependent admittance presented in form of spectrogram (**b**) and 3D visualization (**c**). Note that in plot (**b**) the colourbar is saturated at 4.5 nm/s^2/hPa

$$G_r(\omega) = G(\omega) - \alpha(\omega)P(\omega) \tag{6}$$

Minimising $|G_r(\omega)|^2$ over the whole frequency range leads to:

$$\alpha(\omega) = \frac{\sum G(\omega)P(\omega)}{|P(\omega)|^2} \tag{7}$$

A standard plot of the frequency-dependent admittance obtained with superconducting gravimeters can be found in Hinderer et al. (2014). The distribution of the admittance coefficients between 0 and 12 cpd can be described as a continuous trend where the admittance monotonically increases (in magnitude) from 1.5 to 4 nm s^{-2}/hPa superimposed on a line spectrum with minima at the daily harmonics and sub-harmonics (1, 2, 3,…12 cpd).

The results of the frequency dependent admittance for the gPh#116 at Astroni station are displayed in Fig. 8a. As defined in Eq. (6), it is not surprising that the values of $\alpha(\omega)$ are positive, although the reader should bear in mind that in the time domain there is an inverse correlation between pressure and gravity variations. Obviously, after filtering out the high frequencies, the coefficients are only significant in the range 0–3 cpd. The frequency dependent coefficients are variable in a range between 1 and 6 nms^{-2}/hPa with a mean of about 3.0–3.5 nms^{-2}/hPa; a spectral line is clearly visible with a minimum at the fundamental pressure harmonic at 2 cpd. We also compute the time–frequency barometric admittances by means of a spectrogram approach. In that case the frequency-dependent admittances are computed on a 40-day sliding window with a time shift of 15 days and 0.1 cpd frequency resolution (Fig. 8b). Finally, Fig. 8c offers a 3D vision of Fig. 7b showing a synopsis of the time evolution of the frequency dependent admittances. Even when the latter is considered in conjunction with the spectrogram, it is not possible to investigate any seasonality because of the limited length of the time series.

The main purpose of this detailed study on pressure effects is to verify the 'normal' response of the gravimeter in order to prevent possible biases coming from the atmosphere dynamics in the gravimetric residuals that are our main target of interest. The analysis confirms the suitable quality of gPh#116 observations both in time and frequency domain. We can conclude that, independently on the analysis method used, a consistent and unique value of −3.5 nm/s^2 allows to account for most of the atmospheric pressure effects.

4.3. The Instrumental Drift

We use the gravity data corrected for tides (with the local tidal model derived from the tidal analysis) and after removing tilt and atmospheric effects. Atmospheric effects are modelled employing a unique admittance of −3.5 nm/s^2/hPa.

Figure 9a shows in red the long-term drift of the gPh#116. A minor part of the long-term gravity changes can be ascribed to the caldera long-term uplift (Fig. 9b): in fact during the time-span January-October 2023, the ASTR GNSS station, which is co-located with the gPh#116, recorded a vertical displacement of about 4 cm which can be converted into an equivalent gravity change of about −150 nm/s^2 (Fig. 9a; the local vertical gravity gradient employed is −2900 nm/s^2/m after Berrino et al., 1992) and an average daily drift of −0.5 nm/s^2/day. This is a very small value compared to the actual drift experienced by the gravimeter (compare Figs. 9a and 9b). Excluding such small effect and without the possibility of constraining the trends with absolute gravity observations, we should consider the entire long-term trend as a drift, therefore the effect of ground deformation is included in the drift term. As mentioned in Sect. 3.4, modelling and removing the drift is a critical point for the use of mechanical gravimeters for monitoring active volcanoes, since drift could partially or even totally obliterate Newtonian and/or vertical deformation signals related to the dynamics of volcanic fluids or magmas.

Regarding the drift temporal evolution, at major interruptions the instrument gPh#116 at Astroni has

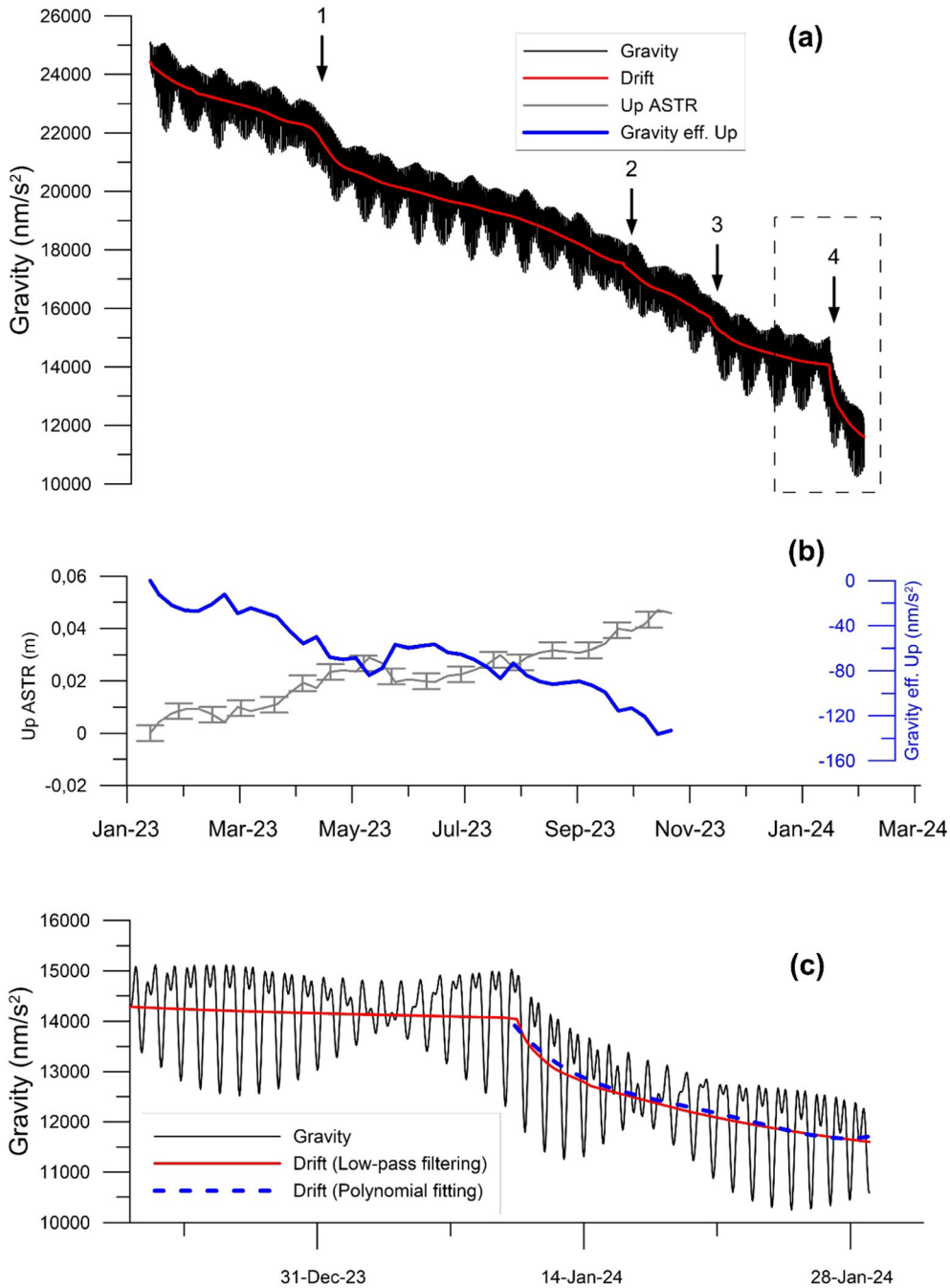

Figure 9

a Gravity record and modelled drift after correction of the main tares (spike, step and gap) due to anthropic (operator maintenance) or natural disturbances (earthquakes). Gaps have been filled with synthetic tide coming from the analysis of the whole dataset and atmospheric contribution assuming a nominal admittance (-3.0 nm s^{-2}/hPa). Numbers and arrows mark the occurrence of the main disturbances (**1**: Power cut after heavy thunderstorm, **2**: Levels Reset, **3**: Power cut after heavy thunderstorm; **4**: Work at the site: use of a percussion hammer next to the gravimeter). **b** time-series of vertical component of the ASTR GNSS station (gray); gravity effect expected at gPh#116 due to the observed uplift (blue curve), assuming a gravity gradient of -2900 nm/s^2/m. Please note the different scale of plot b (blue axes) in comparison with the vertical scale of plot a. **c** Time-series for the period 17th December 2023 -31st January 2024. Drift estimation from low pass filtered gravity data (red curve); approximated drift with a 4th order polynomial after the disturbance (blue dashed line)

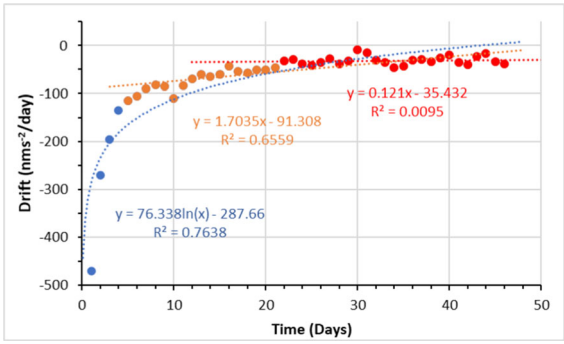

Figure 10
Typical time evolution of the instrumental drift after a main disturbance occurring at the station (time-span analyzed: 10/01/2024- 29/02/2024). The coloured dots represent the drift rate retrieved from a moving windows least-squares regression analysis on gravity residuals (see the main text for more details on the drift computation). Equations represent various fittings of the drift rate observations considering different temporal intervals: blue dotted line exploits the full range of data (0–46 days); orange (5–46 days); red (22–46 days); Day 0 = timing of the disturbance

always shown a *"hockey stick"* drift (see Fig. 9a and 9c).

That is, a high drift rates in the first 4–5 days following the disturbance and then asymptotically tending towards drift values (a few hundreds of nm/s^2/month), typical for this type of instrument designed for recordings. To give a more quantitative overview of this behaviour, the Fig. 10 shows an example of the time evolution of the drift retrieved from a moving window regression analysis on the data collected in the period 10/01/2024- 29/02/2024. In more details, the drift is estimated through a moving window regression in 72-h windows (2880 samples per minute) with 48-h overlap (24 h at the beginning and 24 h at the end of the time-series). The result is a set of slopes of a linear least squares regression fit which represents a drift value every 24 h. The fitting describes the drift rate evolution (Fig. 10): logarithmic trend reproduces quite well the drift rate curve in the whole time-span considered (0–46 days; blue dots in Fig. 10). As it is evident, the drift rate starts becoming nearly linear 4 days after the "disturbing event" (orange dots with related equation in Fig. 10); after 20 days the drift rate is almost constant, as testified by the low daily linear drift rate (0.121 nm/s^2/day^2). In terms of amplitude the drift evolves in the first 4 after the disturbance days from very large (and negative) drift (< -500 nms^{-2}/day) down to values variable in a limited range between -100–150 nms^{-2}/day, finally reaching an asymptotic average value of -50–30 nms^{-2}/day in 10–15 days.

As a result of this behaviour, the appending of the different segments of the record produces time series with very complex trends. The modelling of these trends has required approximations using a piecewise juxtaposition of high-order polynomials or low-pass filtering (LPf): in particular polynomial fitting is employed for the scopes of "residualization" (and also for the atmospheric pressure response study) in order to not suppress completely possible mid-long term signals of interest, while LPf has been used for tidal analysis. In general, the two approaches are quite consistent: for instance, Fig. 9c reports a comparison between the drift modelled using a 4th order polynomial and the LPf version. In both approaches we have a strong reduction of the energy of the residuals by more than 2 orders of magnitude (for the time span considered from about 2500 nm/s^2 to 35 nm/s^2).

4.4. Analysis of Gravity Residuals

Our final gravity residuals consist of the 1-min observations corrected for:

1. tidal effects estimated through the local tidal model.
2. atmospheric pressure changes, modelled with a single admittance of -3.5 nm/s.^{2}
3. tilt effects.
4. drift according to our piecewise polynomial model.

Moreover, in the following analysis we employ both the residuals cleansed by spikes and steps and the "raw" residuals.

A first analysis is performed in order to identify possible hydrological effects on the gravity signal: this is done comparing the "raw" residuals with rainfall records in the area. The rainfall data have been collected by a weather station of University of Naples (DISTAR), located in the eastern sector of the caldera (about 2 km from the station), with 1 -hour sampling rate. We analyze the gravity response

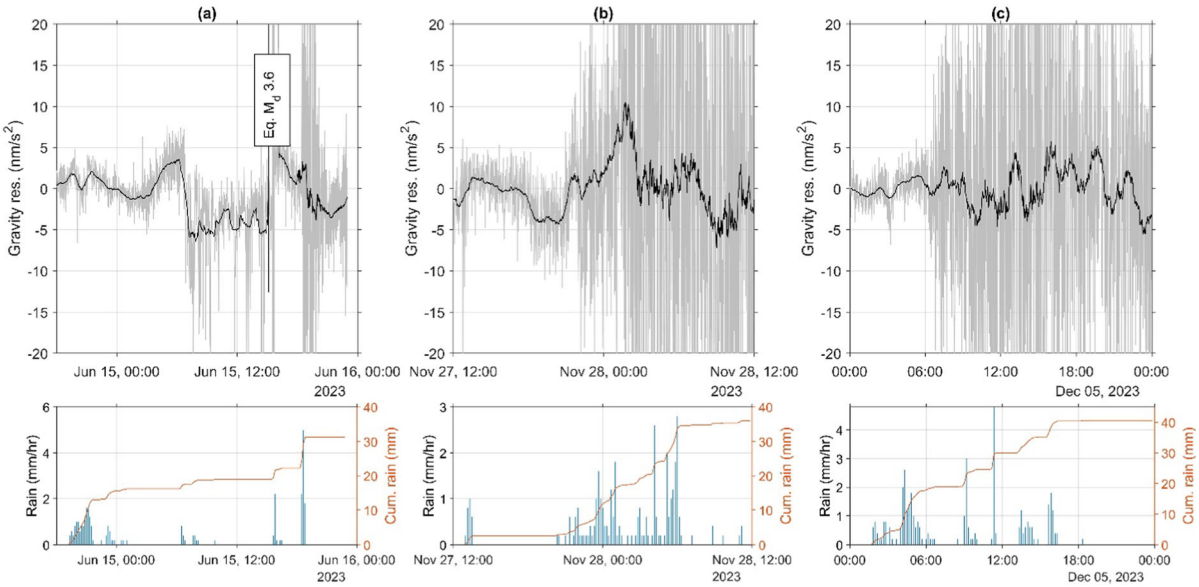

Figure 11
Zoom on gravity residuals in correspondence of three rain events (**a b** and **c**). Top graphs: show the 1-min original residuals (gray) and the low-pass filtered (black). Bottom plots: hourly rain gauge data (blue) and cumulative curve of rain (brown)

during three recharge events driven by heavy rains: one in June 2023 and the other two in November and December. We select events with similar characteristics in terms of cumulative rain and occurring in quiet periods from the point of view of seismicity (except for the event of June 2023).

During rain events the gravity residuals show many high frequency oscillations (gray lines in Fig. 11), in the order of 100 nm/s^2, that can be ascribed to an increase of the noise level owing to bad weather conditions such as vibrations due to wind (see § 4.2). As it is evident from inspection of the time-series (Fig. 11), we do not observe any steps in correspondence of rainfall peaks and no clear gravity variations at lower frequencies related to water mass redistribution during the recharge event. The absence of hydrologic signals could be a consequence of the large shielding of the building, which prevents the accumulation of water in the footprint, the immediate surroundings of the instrument ("*umbrella effect*").

Several steps are observed in the gravity residual time-series (Brownish line of Fig. 12), with amplitudes up to few hundreds of nm/s^2, in occasion of large volcano-tectonic (VT) seismic events (magnitude Md $>$ 2.5) (Fig. 12). The time-lapse gravity data measured during the campaigns in the period 2022–2024 at the co-located benchmark of Astroni is jointly displayed with gravity residuals (Fig. 12a) of the continuous station. Figure 12b displays the time distribution of the VT magnitudes (brown histograms Md $\geq$ 0) as well as the largest ones (blue histograms Md $\geq$ 2.5) are also reported (Surveillance Bulletin INGV-OV, 2023). We observe different gravity steps in correspondence of the largest events. In particular, a step of about 600 nm/s^2 occurred on 18th of August 2023 when, during an intense seismic swarm, three earthquakes with Md $>$ 3.0 were recorded at Solfatara, about 2 km south to Astroni station. We also observe that the amplitude of gravity steps depends on both the magnitude of the VT event and on the distance of the earthquake from the permanent gravity station (Fig. 13): as expected, a positive correlation with magnitude and an inverse relation with the distance event-station turn out.

A further comparison of the continuous gravity observations with the earthquakes occurred during the most intense period of seismic activity (August-October 2023) is reported in Fig. 14. The residual gravity (Fig. 14b) shows different periods of a slight increase (up to about 100 nm/s^2) that are interrupted in correspondence of the larger earthquakes (see for instance the swarm and Md 3.8 events of August and

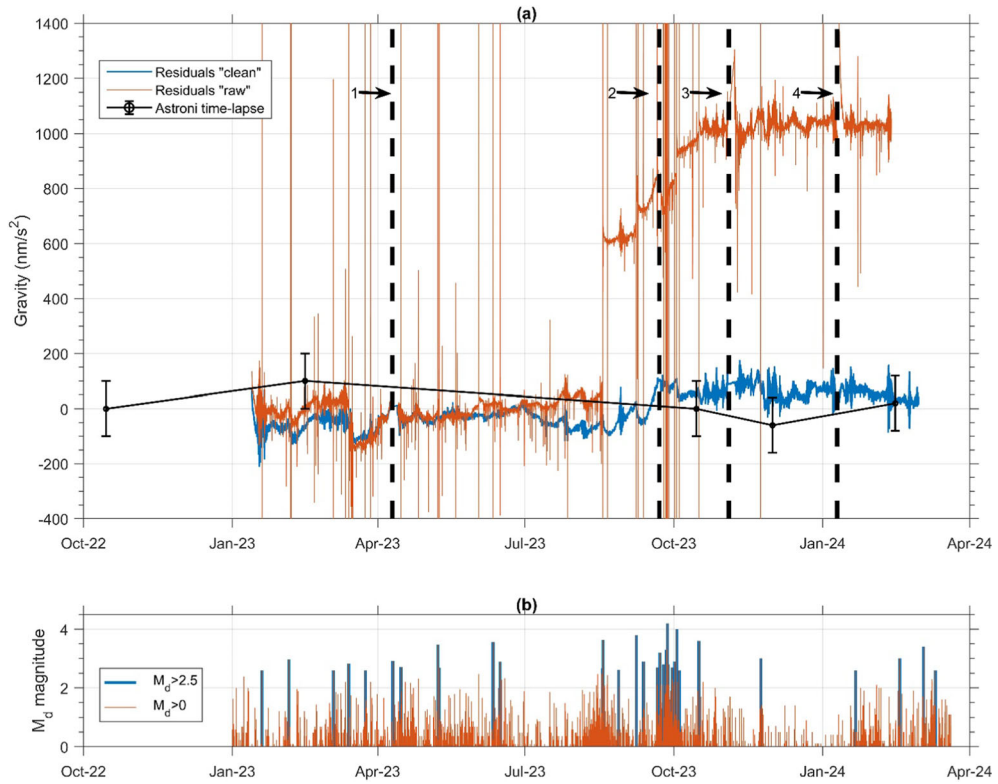

Figure 12

Gravity residuals and seismicity: **a** Blue line: "clean" residuals, after removal of tides, tilt and atmospheric effects, spikes, steps and polynomial drift; Brown line: same as blue, but without correction for steps and spikes; Black line with error bars: gravity variations measured during the time-lapse surveys at the gPh#116 co-located gravity benchmark. Vertical dotted lines report periods of recording interruptions; numbers same as in Fig. 3. **b** Earthquakes with Md $\geq$ 2.5 (blue) and Md $\geq$ 0 (brown) recorded during the observed period (Surveillance Bulletin INGV-OV, 2023; 2024)

September, respectively). It appears that, after these events, the instrument experienced some long-term gravity variations first a rapid gravity decrease followed by a slower and almost linear increase (see for instance the period after 10th September; plots in Fig. 14a). Similar behaviour is also observed in October, after the 4.0 Md event (Fig. 14b); after this event however, we do not observe a clear gravity increase such as in the August–September cases.

5. *Discussion and Conclusions*

5.1. *Quality of Gravity Records and Applied Corrections*

The good agreement with theoretical models of the detected NDFW are clear evidence of the suitable quality of the collected gravity signals, at least in the tidal bands. The tidal analysis confirms that the gPh#116 is well calibrated both in amplitude and phase, as already reported in Riccardi et al. (2023). Furthermore, even if the station is located close to the coast, the quality of the ocean loading correction through the available models is satisfactory. This makes us confident about the reduction of tidal effects on all the gravity measurements collected for volcano monitoring purposes. The response of the gPh#116 to the atmospheric pressure appears to be consistent with theoretical predictions leading us to obtain gravity residuals suitably decorrelated from meteorological effects; gravity residuals also seem uncorrelated to the rainfall.

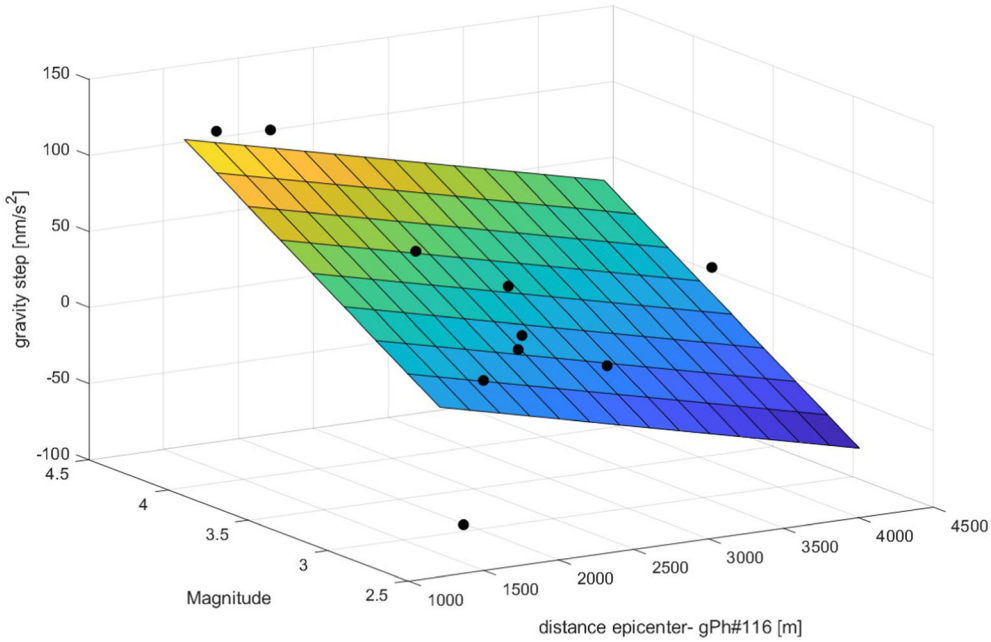

Figure 13
Relationship between gravity step amplitude- earthquake magnitude- distance between epicenter and gPh#116. Best fitting plane is also shown

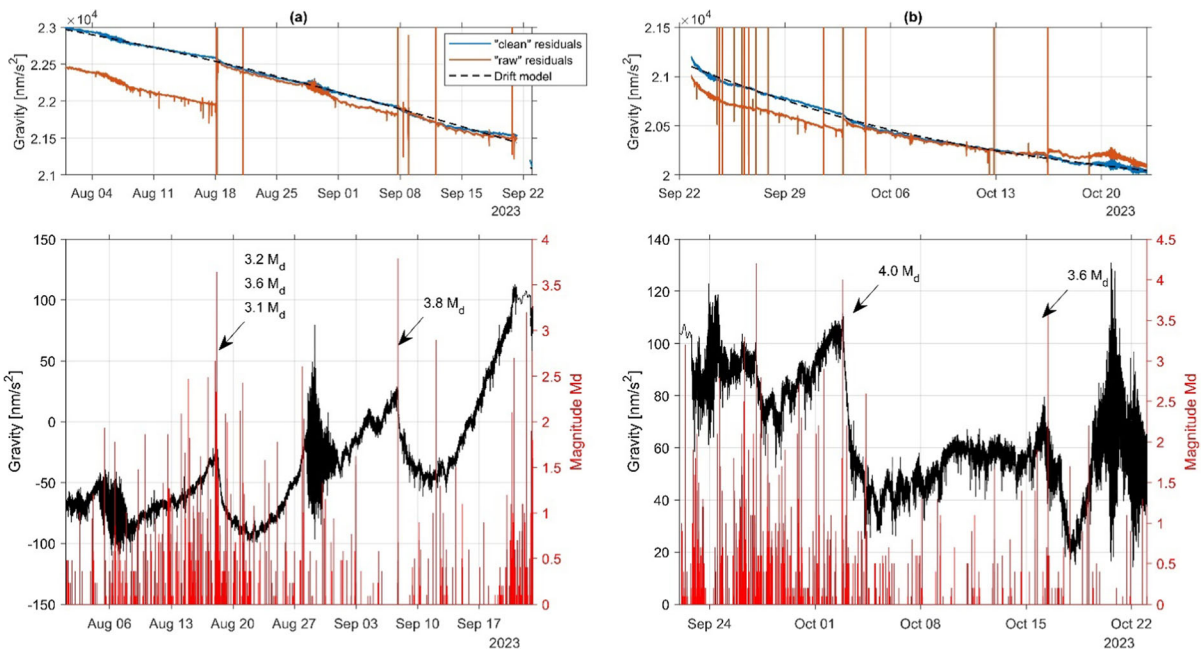

Figure 14
Comparison between gravity residuals and seismicity: zoom on periods August–September (**a**) and October (**b**). In both time-series top graphs report the residual time-series after removal of tides, atmospheric and tilt effects (brown); the residuals after correcting spikes and steps (blue) and the estimated drift (black dashed line). Bottom graphs report the final residuals after removing also the drift (black line) with the catalogue of earthquakes with Md > 0

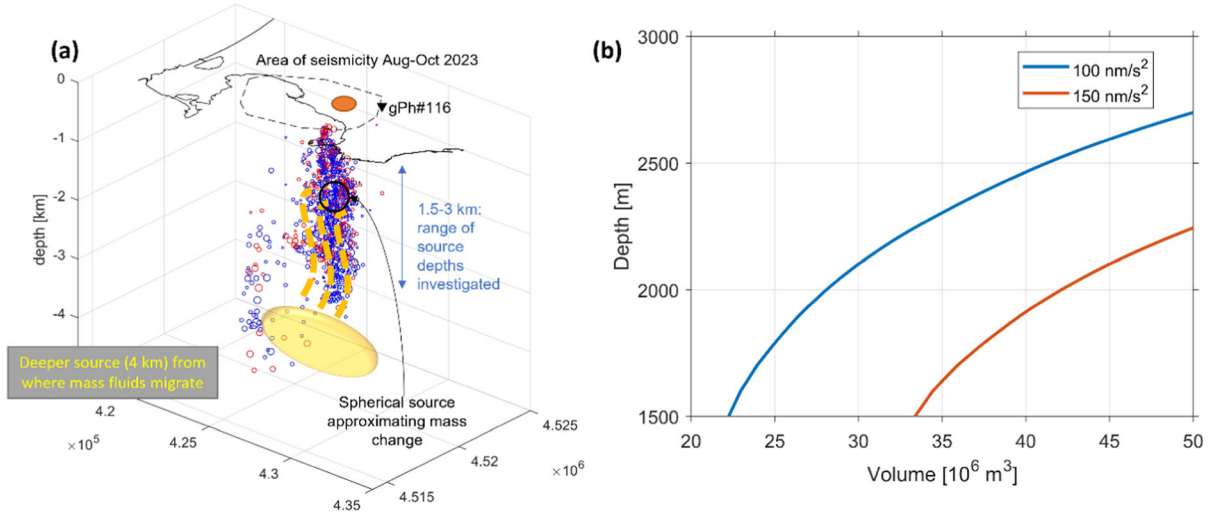

Figure 15

a Sketch that presents the forward modelling tests used to predict the gravity changes at gPh#116 due to a fluid source at Solfatara volcano that rises from a deeper source (4 km) to a shallower level (black circle and azure arrow illustrate the depth range considered). Seismicity of August and September 2023 is shown by red and blue circles respectively (source: Surveillance Bullettin INGV-OV, 2023). Orange circle is the surface projection of the source mass. **b** Forward modelling of fluid sources, located below Solfatara volcano, at different depths and with different volumes producing 100 (blue line) and 150 (red line) nm/s^2 gravity changes at Astroni station gPh#116

5.2. *Possible Gravity Signals Related to Volcano Dynamics at CFc*

As regards the comparison of the gravity variations with the earthquakes at Campi Flegrei, we clearly observe different gravity steps (up to about 600 nm/s^2) concomitantly with seismic events of Md $>$ 2.5. Gravity steps in continuous gravity measurements, due to low-magnitude earthquakes, were even reported at Mt. Etna by Carbone et al. (2009). As mentioned before (see §1), the authors hypothesized that the gravity steps could be geophysical evidence of the dynamical stress transfer between tectonic and magmatic system at local scale. In our case, we can exclude any contribution of volcano-tectonic origin to the observed gravity steps, since the latter are not recorded by the time-lapse survey covering the same period of observation of the gPh#116, at the same location (Fig. 12). Thus, we believe that the recorded steps in gravity signals are likely of instrumental origin (tares), and probably related to the strong shaking experienced by the instrument.

Regarding the gravity transients observed before and after the most energetic VT events and seismic swarms, it is quite challenging to distinguish whether these gravity variations are real (possibly related to fluid migrations) or instrumental effects without any constraint from the absolute gravity measurements. In any case, we can try to discuss some scenarios by quantifying how large should be a mass change located nearby the permanent gravity station to explain such transients in the gravity residuals.

We may consider a mass fluid migration in Solfatara as a possible origin for the gravity changes; this is reasonable given the high temporal correlation with the seismicity and also considering that in the Solfatara area relevant gas fluxes are recorded (Surveillance Bulletin INGV 2024). In this scenario we consider a mass of fluids (with density of 1000 kg/m^3, upper limit for hydrothermal fluid density) that rises from a deeper reservoir (4 km) and reaches a shallower level (1.5–3 km), which corresponds to a depth range where most of the August and September seismicity occurred (Fig. 15a). The horizontal location of such plume corresponds roughly to the Solfatara crater (orange disk in Fig. 15a), located about 1.8 km away from the gPh#116. We compute the gravity effects, assuming a point mass approximation, of both the mass increase

at shallow depth and of the consequent decrease at the deeper reservoir (Fig. 15a).

Under these assumptions, we find that to produce gravity changes of 100–150 nm/s^2 at the gPh#116 location the fluid volume change should be in the order of 10^7 m^3 (Fig. 15b). Smaller volumes are required in case the rising plume reaches the shallower depths: for instance, for an observed gravity increase of 100 nm/s^2, a volume of about 2.2 10^7 m^3 should rise up to 1.5 km depth, while if fluids rising stops at 2.8 km depth, the volume needs to be doubled.

In any case these values appear unreliable since they are in the same order of magnitude of the source volume generating the caldera uplift in the 2011–2013 time interval (Trasatti et al., 2015). Such a rapid (in the order of days) amount of fluid transfer would have induced a detectable transient ground deformation: assuming a Mogi source of overpressure, the expected vertical movements would be in the order of 1 m in the Solfatara area. The NeVoCGNSS stations did not record any signal of such large magnitude. Moreover the time-lapse gravity campaigns, conducted in September–October 2023, did not show any significant gravity variations near the Solfatara benchmark (source: Surveillance Bulletin INGV-OV, 2023).

In conclusion, although we cannot completely rule out the possibility that at least a fraction of these signals may be due to a redistribution of mass in the subsurface, we are inclined to exclude a purely Newtonian origin for these gravity variations, attributing them instead to non-linear drift components, which are not perfectly reproduced by the fitted polynomial model.

5.3. *Implications for Volcano Monitoring from the CF Experience*

In such set up, with a monitoring system relying on spring based instruments, drift remains a critical point for volcano monitoring. Notwithstanding our efforts in modelling the drift by means of high-order polynomials, we do not succeed in retrieving gravity residuals free of instrumental effects. The non-linear response of the meter, in terms of offsets (steps) and exponential drift, owing to the spring relaxation behaviour after strong seismic shakings, limits the usage of such instruments during volcano unrests. In particular, a limiting factor is the detection of mass variations due to fluid/magma migration during intense seismic swarm activity, when inertial disturbances due to the shaking may hide the Newtonian signals. This clearly poses a crucial problem for monitoring in case of rapidly evolving unrests.

The performances of the permanent gravity station could be improved by equipping the instrument with an auto-levelling platform, able to compensate the tilt change associated to most energetic VTs. In our opinion a hybrid gravity approach relying even on time-lapse absolute gravity measurements could contribute to constrain both the time evolution of the long-term as well as the step-like gravity changes.

From our experience, in case of such intense seismic events with an unpredictable timing of occurrence, regularly repeated absolute gravity measurements may not be sufficient to fully recover both the steps and drift changes due to the instrumental response. In case of an energetic VT on the base of our study on the drift evolution (Fig. 10), the optimal repetition of absolute measurements could be: the first as soon as possible after the event (possibly within few hours), then 2 more repetitions after 4–5 and about 10 days after the event. In principle with this set up the user may be able to discriminate the drift term from an eventual Newtonian contribution; however, one has also to consider the different accuracies between absolute and relative instruments, which may further limit the detection of small amplitude gravity transients. Ideally a signal larger than 100 nm/s^2 would be detected by any of the absolute meters presently available (Van Camp et al., 2017).

A further/complementary option is to employ a network of relative time-lapse surveys, on selected loops, as shown in our case in Fig. 12: this has the advantage of a faster measurement protocol, but lower accuracies are expected as well. Hence the threshold of detectability of transient is further increased. Moreover, if only relative observations are collected, the user has to trust the stability of the gravity reference benchmark.

Finally, probably the best option to get rid of the drift terms would be a “superhybrid” approach using

superconducting gravimeters for which drift and mechanical taring is not a major factor.

Acknowledgements

We thank Regione Campania and Dipartimento della Protezione Civile (DPC) for financing the installation and maintenance of Astroni gravity station and WWF Nature Reserve of Astroni for hosting the station. The authors are even grateful to prof. N. Scafetta and Dr. Raffaele Viola from Meteorological Observatory of DiSTAR-UNINA for providing meteorological data, as well as to Dr P. De Martino from INGV-OV for providing the GNSS daily solutions of RITE and ASTR stations. We thank Dr. Craig Miller and Dr. Marvin Reich for detailed reviews and comments which greatly contribute to improve the quality of the paper.

Author Contribution U.R.: conceptualization, investigation, data analysis, first draft writing; T.P.: conceptualization, investigation, data analysis, writing; A.F.: data curation and pre-processing; writing; G.R.: data curation, instrument maintenance; S.C.: conceptualization, investigation, writing;

Funding

Open access funding provided by Istituto Nazionale di Geofisica e Vulcanologia within the CRUI-CARE Agreement. Project PID2019-104726GB-I00/AEI/10.13039/501100011033 of the Spanish Research Agency partially supported this research (U. Riccardi).

Data availability

Data supporting the results of this study are available from the corresponding author [TP] upon reasonable request.

Declarations

Conflict of interest The authors declare no competing interests.

References

Abe, M., Kroner, C., Neumeyer, J., & Chen, X. D. (2010). Assessment of atmospheric reductions for terrestrial gravity observations. *Bulletin d'Information des Marées Terrestres 146*, 11825–11846.

Amoruso, A., Botta, V., & Crescentini, L. (2012). Free Core Resonance parameters from strain data: Sensitivity analysis and results from the Gran Sasso (Italy) extensometers. *Geophysical Journal International, 189*(2), 923–936. https://doi.org/10.1111/j.1365-246X.2012.05440.x

Amoruso, A., Crescentini, L., & Berrino, G. (2008). Simultaneous inversion of deformation and gravity changes in a horizontally layered half-space: Evidences for magma intrusion during the 1982–1984 unrest at Campi Flegrei caldera (Italy). *Earth and Planetary Science Letters, 272*(1–2), 181–188. https://doi.org/10.1016/j.epsl.2008.04.040

Amoruso, A., Crescentini, L., Sabbetta, I., De Martino, P., Obrizzo, F., & Tammaro, U. (2014). Clues to the cause of the 2011–2013 Campi Flegrei caldera unrest, Italy, from continuous GPS data. *Geophysical Research Letters, 41*(9), 3081–3088. https://doi.org/10.1002/2014GL059539

Battaglia, M., Troise, C., Obrizzo, F., Pingue, F., & De Natale, G. (2006). Evidence for fluid migration as the source of deformation at Campi Flegrei caldera (Italy). *Geophysical Research Letters*.https://doi.org/10.1029/2005GL024904

Berrino, G. (1994). Gravity changes induced by height-mass variations at the Campi Flegrei caldera. *Journal of Volcanology and Geothermal Research, 61*(3–4), 293–309. https://doi.org/10.1016/0377-0273(94)90010-8

Berrino, G., Rymer, H., Brown, G. C., & Corrado, G. (1992). Gravity-height correlations for unrest at calderas. *Journal of Volcanology and Geothermal Research, 53*(1–4), 11–26. https://doi.org/10.1016/0377-0273(92)90071-K

Bonafede, M., Amoruso, A., Crescentini, L., Gottsmann, J. H., Todesco, M., & Trasatti, E. (2022). Source modelling from ground deformation and gravity changes at the Campi Flegrei Caldera, Italy. In G. Orsi, M. D'Antonio, & L. Civetta (Eds.), *Campi Flegrei: A Restless Caldera in a Densely Populated Area* (pp. 283–309). Berlin: Springer.

Bos, M., & Scherneck, H-G. (2023). Free ocean tide loading provider. http://holt.oso.chalmers.se/loading/. Accessed 14 Feb 2024.

Boy, J.-P., & Chao, B. F. (2005). Precise evaluation of atmospheric loading effects on Earth's time-variable gravity field. *Journal of Geophysical Research, 110*, B08412. https://doi.org/10.1029/2002JB002333

Buono, G., Paonita, A., Pappalardo, L., Caliro, S., Tramelli, A., & Chiodini, G. (2022). New insights into the recent magma dynamics under Campi Flegrei caldera (Italy) from petrological and geochemical evidence. *Journal of Geophysical Research: Solid Earth, 127*(3), e2021JB023773. https://doi.org/10.1029/2021JB023773

Carbone, D., Jousset, P., & Musumeci, C. (2009). Gravity "steps" at Mt. Etna volcano (Italy): Instrumental effects or evidences of earthquake-triggered magma density changes? *Geophysical Research Letters*. https://doi.org/10.1029/2008GL036179

Carbone, D., Cannavò, F., Montagna, C. P., & Greco, F. (2023). Gas buffering of magma chamber contraction during persistent explosive activity at Mt. *Etna Volcano. Communications Earth & Environment, 4*(1), 471. https://doi.org/10.1038/s43247-023-01149-x

Carbone, D., Zuccarello, L., & Saccorotti, G. (2008). Geophysical indications of magma uprising at Mt Etna during the December 2005 to January 2006 non-eruptive period. *Geophysical Research Letters, 35*, L06305. https://doi.org/10.1029/2008GL033212

Carbone, D., Zuccarello, L., Saccorotti, G., & Greco, F. (2006). Analysis of simultaneous gravity and tremor anomalies observed during the 2002–2003 Etna eruption, *Earth Planet. Sci. Lett., 245*, 616–629. https://doi.org/10.1016/j.epsl.2006.03.055

Carlino, S. (2019). Volcanoes and risk. In S. Carlino (Ed.), *Neapolitan Volcanoes A Trip Around Vesuvius, Campi Flegrei and Ischia.* Cham: Springer International Publishing.

Carrere, L., Lyard, F., & Cancet, M. (2015). FES2014, a new tidal model on the global ocean with enhanced accuracy in shallow seas and in the arctic region. EGU general assembly (pp. 12–17) April Vienna (Austria).

Chiodini, G., Caliro, S., Avino, R., Bini, G., Giudicepietro, F., Cesare, W. D., Ricciolino, P., Aiuppa, A., Cardellini, C., Petrillo, Z., Selva, J., Siniscalchi, A., & Tripaldi, S. (2021). Hydrothermal pressure-temperature control on CO2 emissions and seismicity at Campi Flegrei (Italy). *Journal of Volcanology and Geothermal Research, 414*, 107245.

Crossley, D., Hinderer, J., & Rosat, S. (2002). Using the atmosphere–gravity correlationto derive a time-dependent admittance. *Bull. D'inf. Marées Terr., 136*, 10809–10820.

Cui, X., Sun, H., Xu, J., Zhou, J., & Chen, X. (2018). Detection of free core nutation resonance variation in Earth tide from global superconducting gravimeter observations. *Earth, Planets and Space, 70*(1), 1–12. https://doi.org/10.1186/s40623-018-0971-9

D'Auria, L., Pepe, S., Castaldo, R., Giudicepietro, F., Macedonio, G., Ricciolino, P., & Zinno, I. (2015). Magma injection beneath the urban area of Naples: a new mechanism for the 2012–2013 volcanic unrest at Campi Flegrei caldera. *Scientific Reports, 5*(1), 13100. https://doi.org/10.1038/srep13100

Danesi, S., Pino, N. A., Carlino, S., & Kilburn, C. R. (2024). Evolution in unrest processes at Campi Flegrei caldera as inferred from local seismicity. *Earth and Planetary Science Letters, 626*, 118530. https://doi.org/10.1016/j.epsl.2023.118530

De Martino, P., Dolce, M., Brandi, G., Scarpato, G., & Tammaro, U. (2021). The ground deformation history of the Neapolitan volcanic area (Campi Flegrei Caldera, Somma-Vesuvius Volcano, and Ischia Island) from 20 years of continuous GPS observations (2000–2019). *Remote Sens, 13*(14), 2725. https://doi.org/10.3390/rs13142725

De Martino, P., Guardato, S., Donnarumma, G. P., Dolce, M., Trombetti, T., Chierici, F., & Iannaccone, G. (2020). Four years of continuous seafloor displacement measurements in the Campi Flegrei caldera. *Frontiers in Earth Science, 8*, 615178. https://doi.org/10.3389/feart.2020.615178

Dehant, V., Defraigne, P., & Wahr, J. (1999). Tides for a convective Earth. *Journal of Geophysical Research, 104*(B1), 1035–1058. https://doi.org/10.1029/1998JB900051

Dehant, V., & Zschau, J. (1989). The effect of mantle inelasticity on tidal gravity: A comparison between the spherical and the elliptical Earth model. *Geophysical Journal International, 97*(3), 549–555. https://doi.org/10.1111/j.1365-246X.1989.tb00522.x

Del Gaudio, C., Aquino, I., Ricciardi, G. P., Ricco, C., & Scandone, R. (2010). Unrest episodes at Campi Flegrei: A reconstruction of vertical ground movements during 1905–2009. *Journal of Volcanology and Geothermal Research, 195*, 48–56.

Del Pezzo, E., De Natale, G., Martini, M., & Zollo, A. (1987). Source parameters of microearthquakes at Phlegraean Fields (Southern Italy) volcanic area. *Phys Earth Planet Int, 47*, 25–42. https://doi.org/10.1016/0031-9201(87)90064-1

Ducarme, B., & Schüller, K. (2018). Canonical wave grouping as the key to optimal tidal analysis. *Bulletin D'informations Marees Terrestres, 150*, 12131.

Eanes, R., (2002). The CSR4.0 global ocean tide model. ftp://www.csr.utexas.edu/pub/tide

Egbert, G. D., & Erofeeva, L. (2002). Efficient inverse modeling of barotropic ocean tides. *Journal of the Seismological Society of Japan, 19*(2), 183–204. https://doi.org/10.1175/1520-0426(2002)019%3c0183:EIMOBO%3e2.0.CO;2

Farrell, W. E. (1972). Deformation of the earth by surface loads. *Reviews of Geophysics, 10*(3), 761–797. https://doi.org/10.1029/RG010i003p00761

Fok, H. S. (2012). Ocean tides modeling using satellite altimetry. Geodetic Science Report No.501, Ohio State University

Fores, B., Klein, G., Le Moigne, N., & Francis, O. (2019). Long-term stability of tilt-controlled gPhoneX gravimeters. *Journal of Geophysical Research: Solid Earth, 124*(11), 12264–12276. https://doi.org/10.1029/2019JB018276

Forster, F., Güntner, A., Jousset, P., Reich, M., Männel, B., Hinderer, J., & Erbas, K. (2021). Environmental and anthropogenic gravity contributions at the Þeistareykir geothermal field North Iceland. *Geothermal Energy, 9*, 26. https://doi.org/10.1186/s40517-021-00208-w

Gottsmann, J., Folch, A., & Rymer, H. (2006a). Unrest at Campi Flegrei: A contribution to the magmatic versus hydrothermal debate from inverse and finite element modeling. *Journal of Geophysical Research: Solid Earth*. https://doi.org/10.1029/2005JB003745

Gottsmann, J., Rymer, H., & Berrino, G. (2006b). Unrest at the Campi Flegrei caldera (Italy): A critical evaluation of source parameters from geodetic data inversion. *Journal of Volcanology and Geothermal Research, 150*(1–3), 132–145. https://doi.org/10.1016/j.jvolgeores.2005.07.002

Hart-Davis, M. G., Piccioni, G., Dettmering, D., Schwatke, C., Passaro, M., & Seitz, F. (2020). EOT20: A global ocean tide model from multi-mission satellite altimetry. *Earth Syst Sci Data, 13*, 3869–3884. https://doi.org/10.5194/essd-13-3869-2021

Hector, B., Hinderer, J., Seguis, L., Boy, J.-P., Calvo, M., Descloitres, M., Rosat, S., Galle, S., & Riccardi, U. (2014). Hydro-gravimetry in West-Africa: First results from the Djougou (Benin) superconducting gravimeter. *Journal of Geodynamics, 80*, 34–49. https://doi.org/10.1016/j.jog.2014.04.003

Hinderer, J., Hector, B., Boy, J. P., Riccardi, U., Rosat, S., Calvo, M., & Littel, F. (2014). A search for atmospheric effects on gravity at different time and space scales. *Journal of Geodynamics, 80*, 50–57. https://doi.org/10.1016/j.jog.2014.02.001

Huang, N. E., Shen, Z., Long, S. R., Wu, M. C., Shih, H. H., Zheng, Q., & Liu, H. H. (1998). The empirical mode decomposition and the Hilbert spectrum for nonlinear and non-stationary time series analysis. *Proceedings of the Royal Society of London Series a: Mathematical Physical and Engineering Sciences, 454*(1971), 903–995. https://doi.org/10.1098/rspa.1998.0193

Hugill, A. (2021). Gravimeters. In H. K. Gupta (Ed.), *Encyclopedia of Solid Earth Geophysics* (pp. 578–585). Cham: Springer International Publishing.

Iida, K., Hayakawa, M., & Katayose, K. (1952). Gravity survey of Mihara volcano, Ooshima Island, and changes in gravity caused by eruption. Geological Survey of Japan.

Jousset, P., Dwipa, S., Beauducel, F., Duquesnoy, T., & Diament, M. (2000). Temporal gravity at Merapi during the 1993–1995 crisis: An insight into the dynamical behaviour of volcanoes. *Journal of Volcanology and Geothermal Research, 100*, 289–320. https://doi.org/10.1016/S0377-0273(00)00141-4

Micro-g LaCoste, Inc. (2013). gPhoneX Hardware Manual V3.1., http://microglacoste.com/wp-content/uploads/2017/06/gPhoneXmanual.pdf Accessed 10 Feb 2024

Long, L. T., & Kaufmann, R. D. (2013). Instruments and data reductions, In: *Acquisition and analysis of terrestrial gravity data*. Cambridge University Press, pp. 171

Matsumoto, K., Takanezawa, T., & Ooe, M. (2000). Ocean tide models developed by assimilating TOPEX/POSEIDON altimeter data into hydrodynamical model: A global model and a regional model around Japan. *J. of Oceanog., 56*, 567–581. https://doi.org/10.1023/A:1011157212596

Merriam, J. B. (1994). The nearly diurnal free wobble resonance in gravity measured at Cantley. *Quebec. Geophysical Journal International, 119*(2), 369–380. https://doi.org/10.1111/j.1365-246X.1994.tb00129.x

Meurers, B. (2024). Correction of high-frequency (> 03 mHz) air pressure effects in gravity time-series. *Geophysical Journal International, 237*(1), 14–30. https://doi.org/10.1093/gji/ggae030

Moretti, R., De Natale, G., & Troise, C. (2020). Hydrothermal versus magmatic: geochemical views and clues into the unrest dilemma at Campi Flegrei. In *Vesuvius, Campi Flegrei, and Campanian Volcanism*. Elsevier pp. 371–406

Mouyen, M. (2023). Strategies to remove hydrological effects in continuous gravity time series. *Journal of Geodesy, 97*(10), 91. https://doi.org/10.1007/s00190-023-01785-3

Niebauer, T. (1988). Correcting gravity measurements for the effects of local air pressure. *Journal of Geophysical Research, 93*(B7), 7989–7991. https://doi.org/10.1029/JB093iB07p07989

Petrosino, S., De Siena, L., & Del Pezzo, E. (2008). Recalibration of the Magnitude Scales at Campi Flegrei, Italy, on the basis of measured path and site and transfer functions recalibration of the magnitude scales at Campi Flegrei. *Italy B Seismol Soc Am, 98*, 1964–1974. https://doi.org/10.1785/0120070131

Pivetta, T., Riccardi, U., Ricciardi, G., & Carlino, S. (2023). Hydrological and volcano-related gravity signals at Mt. Somma–Vesuvius from ~ 20 yr of time-lapse gravity monitoring: implications for volcano quiescence. Geophysical Journal International. 235(2):1565–1580. https://doi.org/10.1093/gji/ggad320

Pivetta, T., Braitenberg, C., Gabrovšek, F., Gabriel, G., & Meurers, B. (2024). Gravimetry and hydrologic data to constrain the hydrodynamics of a karstic area: The Škocjan Caves study case. *Journal of Hydrology, 629*, 130453. https://doi.org/10.1016/j.jhydrol.2023.130453

Polcari, M., Borgstrom, S., Del Gaudio, C., De Martino, P., Ricco, C., Siniscalchi, V., & Trasatti, E. (2022). Thirty years of volcano geodesy from space at Campi Flegrei caldera (Italy). *Scientific Data, 9*(1), 728. https://doi.org/10.1038/s41597-022-01849-7

Portier, N., Hinderer, J., Riccardi, U., Ferhat, G., Calvo, M., Abdelfettah, Y., & Bernard, J.-D. (2018). Hybrid gravimetry monitoring of Soultz-sous-Forêts and Rittershoffen geothermal sites (Alsace, France). *Geothermics, 76*, 201–219. https://doi.org/10.1186/s40517-018-0104-5

Riccardi, U., Boy, J. P., Hinderer, J., Rosat, S., & Boudin, F. (2016). Free Core Nutation parameters from hydrostatic long-base tiltmeter records in Sainte Croix aux Mines (France). In J. T. Freymueller & L. Sánchez (Eds.), *International Symposium on Earth and Environmental Sciences for Future Generations: Proceedings of the IAG General Assembly, Prague, Czech Republic, June 22–July 2, 2015* (pp. 171–179). Cham: Springer International Publishing.

Riccardi, U., Carlino, S., Pivetta, T., Hinderer, J., Rosat, S., & Ricciardi, G. (2023). Continuous gravity observations at Mt. Somma-Vesuvius with a gPhoneX Gravimeter: In-depth instrumental response characterization and tidal model. *Pure and Applied Geophysics, 180*(7), 1–26. https://doi.org/10.1007/s00024-023-03313-y

Riccardi, U., Berrino, G., Corrado, G., & Hinderer, J. (2008). Strategies in the processing and analyses of continuous gravity record in active volcanic areas: The case of Mt.Vesuvius. *Annals of Geophysics, 51*, 67–85. https://doi.org/10.4401/ag-3039

Riccardi, U., Hinderer, J., & Boy, J. P. (2007). On the efficiency of barometric arrays to improve the reduction of atmospheric effects on gravity data. *Physics of the Earth and Planetary Interiors, 161*(3–4), 224–242. https://doi.org/10.1016/j.pepi.2007.02.007

Rosat, S., & Lambert, S. B. (2009). Free core nutation resonance parameters from VLBI and superconducting gravimeter data. *Astronomy & Astrophysics, 503*(1), 287–291. https://doi.org/10.1051/0004-6361/200811489

Sainz-Maza Aparicio, S., Arnoso Sampedro, J., González Montesinos, F., & Martí Molist, J. (2014). Volcanic signatures in time gravity variations during the volcanic unrest on El Hierro (Canary Islands). *Journal of Geophysical Research: Solid Earth, 119*(6), 5033–5051. https://doi.org/10.1002/2013JB010795

Schüller, K. (2020). Theoretical basis for earth tide analysis and prediction. Manual-01-ET34-X-V, Surin, Thailand, PP. 217.

Spratt, R. S. (1982). Modelling the effect of atmospheric pressure variations on gravity. *Geophysical Journal of the Royal Astronomical Society, 71*(1), 173–186. https://doi.org/10.1111/j.1365-246X.1982.tb04991.x

Sugihara, M., Nawa, K., Nishi, Y., Ishido, T., & Soma, N. (2013). Continuous gravity monitoring for CO2 geo-sequestration. *Energy Procedia, 37*, 4302–4307. https://doi.org/10.1016/j.egypro.2013.06.333

Surveillance Bullettin INGV-OV (2023): https://www.ov.ingv.it/index.php/monitoraggio-e-infrastrutture/bollettini-tutti/mensili-dei-vulcani-della-campania/flegrei/anno-2023-1

Surveillance Bullettin INGV-OV (2024): https://www.ov.ingv.it/index.php/monitoraggio-e-infrastrutture/bollettini-tutti/mensili-dei-vulcani-della-campania/flegrei/anno-2024-1

Wenzel, H. G. (1996). The nanogal software: earth tide data processing package. *Marees Terrestres Bulletin Informations, 124*, 9425–9439.

Trasatti, E., Bonafede, M., Ferrari, C., Giunchi, C., & Berrino, G. (2011). On deformation sources in volcanic areas: Modeling the Campi Flegrei (Italy) 1982–84 unrest. *Earth and Planetary Science Letters, 306*(3–4), 175–185. https://doi.org/10.1016/j.epsl.2011.03.033

Trasatti, E., Polcari, M., Bonafede, M., & Stramondo, S. (2015). Geodetic constraints to the source mechanism of the 2011–2013 unrest at Campi Flegrei (Italy) caldera. *Geophysical Research Letters, 42*(10), 3847–3854. https://doi.org/10.1002/2015GL063621

Van Camp, M., & Vauterin, P. (2005). Tsoft: Graphical and interactive software for the analysis of time series and Earth tides. *Computers & Geosciences, 31*(5), 631–640. https://doi.org/10.1016/j.cageo.2004.11.015

Van Camp M., de Viron, O., Watlet, A., Meurers, B., Francis, O., & Caudron, C. (2017). Geophysics from terrestrial time-variable gravity measurements. *Reviews of Geophysics, 55*(4), 938–992. https://doi.org/10.1002/2017RG000566

Wahr, J. M., & Bergen, Z. (1986). The effects of mantle anelasticity on nutations, Earth tides, and tidal variations in rotation rate. *Geophysical Journal of the Royal Astronomical Society, 64*, 633–668. https://doi.org/10.1111/j.1365-246X.1986.tb06642.x

Williams-Jones, G., Rymer, H., Mauri, G., Gottsmann, J., Poland, M., & Carbone, D. (2008). Toward continuous 4D microgravity monitoring of volcanoes. *Geophysics, 73*(6), WA19–WA28. https://doi.org/10.1190/1.2981185

de Zeeuw-van Dalfsen, E., & Poland, M. P. (2023). Microgravity as a tool for eruption forecasting. *Journal of Volcanology and Geothermal Research*. https://doi.org/10.1016/j.jvolgeores.2023.107910

(Received May 7, 2024, revised July 9, 2024, accepted August 7, 2024)